Frisbee Flight Simulation and Throw Biomechanics

By

SARAH ANN HUMMEL
B.S. (University of Missouri, Rolla) 1997

THESIS

Submitted in partial satisfaction of the requirements for the degree of

MASTER OF SCIENCE

in

Mechanical Engineering

in the

OFFICE OF GRADUATE STUDIES

of the

UNIVERSITY OF CALIFORNIA

DAVIS

Approved:

_____

_____

_____

Committee in Charge

2003

Table of contents

iii

List of Figures

List of Tables

Acknowledgements

Preface

This thesis documents the work of two separate projects, Frisbee Flight Simulation and Frisbee Throw biomechanics. Chapter 1 provides an overall introduction to the entire project. The research then follows as three stand-alone chapters, Chapters 2, 3 and 4, prepared for journal submission. Some redundancy, mostly in the introduction sections does occur. The appendix following the references includes selected MATLAB and AUTOLEV code.

NOTE: The word Frisbee and disc are used interchangeably throughout the text. Frisbee is a registered trademarked name of Wham-O Manufacturing.

Nomenclature

A	Frisbee planform area (m^2)
COM	center of mass
COP	center of pressure
d	diameter of Frisbee (m)
D	drag force (N)
DOF	degree of freedom
C_D	drag coefficient
C_{D0}	form drag coefficient at minimum drag, $\alpha = \alpha_o$
$C_{D\alpha}$	induced drag coefficient, dependent on α
C_L	lift coefficient
C_{Lo}	lift coefficient at $\alpha = 0$
$C_{L\alpha}$	lift coefficient dependent on α
C_M	pitch moment coefficient
C_{Mo}	pitch moment coefficient at $\alpha = 0$
$C_{M\alpha}$	pitch moment coefficient dependent on α
C_{Mq}	pitch moment damping coefficient
C_{Nr}	spin down moment coefficient
C_{Rr}	roll moment damping due to spin coefficient
C_{Rp}	roll moment damping coefficient
F	sum of aerodynamic forces
H, $\dot{H}$	angular momentum, rate of change of angular momentum
I_{xx}, I_{yy}	Frisbee diametrial moment of inertia
I_{zz}	Frisbee axial moment of inertia
L	lift force (N)
m	Frisbee mass (kg)
mg	weight, gravity force (N)
M	sum of aerodynamic moments
$p\left(\omega_x\right), q\left(\omega_y\right), r\left(\omega_z\right)$	roll, pitch, and yaw rates (rad/s)
$\dot{p}\left(\dot{\omega}_x\right), \dot{q}\left(\dot{\omega}_y\right), \dot{r}\left(\dot{\omega}_z\right)$	roll, pitch, and yaw angular accelerations (rad/s^2)
R, M, N	roll, pitch, spin down moments (N m)
r	radius of Frisbee (m)
Re	Reynolds number
S	spin parameter ($r\omega_z /v$)
v	velocity (m/s)
x, y, z	roll, pitch, yaw axes
α	angle of attack
α_0, $\alpha_{eq} = - C_{Lo} / C_{L\alpha}$	angle of attack at zero lift and minimum drag
β	angle between velocity vector and horizontal
ϕ, θ, γ	123 Euler angle rotations, roll, pitch, yaw respectively
ρ	air density
$\dot{\Psi}$	precession rate
μ	dynamic viscosity
ω	total angular velocity of Frisbee

Chapter 1   Introduction

1.1   Frisbee History

The first plastic Frisbee was created in the 1940's and now over 50 companies produce flying discs of varying size and weight. More flying discs are sold each year than baseballs, basketballs, and footballs combined (Wham-O.com). Frisbee appeal has exploded from a mere recreational toy to spawn numerous international sports including Ultimate Frisbee, Disc Golf and Freestyle. Its popularity stems from the aerodynamic characteristics that allow a variety of maneuvers and flight paths, all relatively easy for a new thrower to learn. International governing bodies such as the Professional Disc Golf Association and the World Flying Disc Federation promote the development and advancement of Frisbee games, culminating in the appearance of Ultimate and Disc Golf in the 2001 World Games in Akita Japan as full medal sports.

Walter Morrison and Ed Headrick each played a defining role in the evolution of the Frisbee. Morrison manufactured the first disc in 1948, improving his design in 1951 to produce the Pluto Platter. Wham-O teamed up with Morrison in 1957 and began mass production. Inspired by a trip to Ivy League campuses, Wham-O executives renamed their discs "Frisbees" and currently hold the trademarked name. Other manufacturers make discs, but only Wham-O makes Frisbees. Ed Headrick served as executive Vice President, General Manager and CEO of Wham-O over a ten year period. His major contributions stem from his vision to expand Frisbee to more than just a game of catch. He experimented with the design and in 1965 filed his new Frisbee model with the US patent Office, vastly improving the stability of the Frisbee. Founder of the International

Frisbee Association, he promoted and organized various Frisbee sport competitions throughout the United States, remaining active up until his death in 2002.

Prior to plastic, Frisbee's did exist in a somewhat similar but metallic form. As early as the 1920's, Yale students flung their left over pie tins to each other across cafeterias and campuses. The pin tins bore the stamp "Frisbie Pies" for the name of the manufacturer, the Frisbie Pin Tin Company. Other claims exist also regarding "who threw the first disc", some even jokingly tracing the earliest origins to the 450 B.C. statue of Discobolus.

1.2   Frisbee Literature

Interest in Frisbees has extended well beyond the athletic fields. Frisbee: A Practitioner's Manual and Definitive Treatise, by Johnson (1975) is still a valuable resource, including information on the history of the Frisbee, Frisbee game regulations and throwing techniques. Several books document basic throwing techniques (Johnson, 1975; Roddick, 1980; Tips, 1977). Cotroneo (1980) compared the force contribution of body segments in backhand versus forehand Frisbee throws, while inquisitive athletes have qualitatively investigated optimal throwing form, videotaping throwing events to record corresponding Frisbee speed and flight distance (Pozzy, 2002). However, as Frisbee sports have grown and the drive to advance throwing skills has continued, quantitative Frisbee throw biomechanics have been neglected.

Two brief, somewhat anecdotal, descriptions of the flight dynamics and aerodynamics for the informed layman have been provided by Bloomfield (1999) and Schuurmans (1990). Until recently scientific, quantitative research on Frisbee flight mechanics was relatively scarce. In 1972 the U.S. Navy commissioned a project in which Stilley (1972) investigated a self-suspended Frisbee-like flare. He used wind tunnel studies to measure the aerodynamic lift and drag on the Frisbee as a function of angle of attack, α, the angle between the velocity vector and the Frisbee plane. Spinning and non-spinning wind tunnel tests showed that the effect of spin on aerodynamic forces and moments is small. Stilley & Carstens (1972) analyzed flight stability and compared actual flights to free-fall tests.

Several other wind tunnel studies have been performed within the last 5 years. Mitchell (1999) measured Frisbee lift and drag on non-spinning discs. Yasuda (1999) measured lift and drag for a range of flow speeds and spin rates for Frisbees and flat plates. Potts and Crowther (2000; 2001; 2002) have performed an exhaustive series of wind tunnel tests measuring not only lift and drag but also pitching and rolling moments. Additionally they have analyzed pressure distribution and air flow around the Frisbee. They verified the results of Stilley that spin effects, although observable, are not overly important in the generation of aerodynamic forces.

Lissaman (1993) investigated the flight stability of an oblate spheroid by considering the effect of each stability derivative (aerodynamic coefficient) on the characteristic equation. He has also studied maximum range flight.

1.3 Research Overview

This research aims to model the flight of the Frisbee to enable simulation of the trajectory for any set of initial release conditions. How a person might produce these release conditions (with the goal of someday being able to throw further) is the goal of a separate but related Frisbee biomechanics study.

A dynamic model for Frisbee flight mechanics is proposed. The forces and the moments acting on the Frisbee and how they interplay with the spin to control the flight are described in detail in Chapter 2: Dynamics of the Disc. What remains is to calculate the magnitudes of these forces and moments so that the trajectory of the flight can be determined. This calculation is dependent on obtaining values for the 10 aerodynamic coefficients included in the force and moment equations. Chapter 3 is a detailed discussion of the experimental set-up and analysis to estimate these coefficients. But before the Frisbee has a trajectory, it must be set into motion. Chapter 4 presents a biomechanical throwing model to understand how a thrower generates the power to release the Frisbee.

Chapter 2   Dynamics of the Disc

2.1   Introduction

The Frisbee is both an airfoil and a gyroscope. Understanding the flight of a Frisbee

requires analyzing how the two systems interact. This knowledge can then be used to

critically analyze flight patterns. The following discussion focuses on the basic dynamic

principles, without reflecting on the specific implications of the complicated air flow and

pressure distribution on Frisbee flight. The values of parameters refer to studies

performed on a 0.175 kg Discraft Ultrastar. The basic theories apply to other Frisbees,

but the parameters will vary as will the relative magnitude of a given force or moment.

All throws discussed are right hand backhand throws, such that the spin of the Frisbee is

clockwise viewed from above. The Frisbee reference frame F is a set of principal axes

(not fixed in the body) with origin at the mass center (Fig.2-1c). The x axis is generally

forward, aligned with the projection of the velocity vector on the disc plane. The z axis is

the axis of symmetry, perpendicular to the Frisbee plane. The y axis is also in the plane of

the Frisbee, $y = z \times x$. The x and y axes are not body fixed and thus do not rotate with the

Frisbee spin about the vertical axis of symmetry z, although they will rotate slowly as the

direction of the velocity changes.

2.2 Airfoil

Gravitational and aerodynamic forces act on the Frisbee during flight to accelerate the disc according to Newton's Law

$$\mathbf{F}=m\mathbf{a} \tag{2.1}$$

The aerodynamic forces change continually throughout flight, as may the orientation of the disc in inertial space and the angle of attack, α, the angle between the plane of the Frisbee and the relative velocity vector. (Fig. 2-1a)

2.2.1 Gravity

Gravity is a constant vertical force. It is not dependent on speed or angle of attack. It acts at the center of mass to pull the Frisbee to the ground.
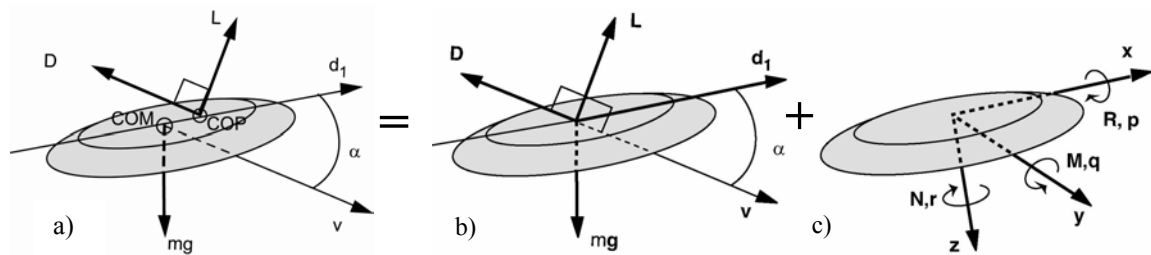
Figure 2-1 Forces and moments on a falling disc, a) and b) + c) are equivalents systems. a) Center of pressure (COP) and center of mass (COM) are not coincident. b) Drag **D** and lift **L** act opposite and perpendicular to the velocity v, respectively, and in a place perpendicular to the disc plane. They are primarily functions of the velocity and angle of attack, α, the angle between **v** and **d₁** in the disc plane. c) xyz axes of the disc; roll **R**, pitch **M** and spin down **N** moments; roll p, pitch q and yaw r angular velocities.

2.2.2 Aerodynamic Forces

The aerodynamic forces include drag and lift. They are both roughly quadratic in velocity, are strong functions of α, and act at the center of pressure. However the center of pressure (COP) is not necessarily coincident with the center of mass (COM), nor is it constant. Therefore aerodynamic moments are induced which cause angular accelerations

6

and precession and have an affect on the wobble of the disc during flight. Figure 2-1a illustrates the forces acting on a Frisbee while Figs. 2-1b and 2-1c illustrate an equivalent system where the lift and drag at the COP have been replaced by equal parallel forces at the COM plus moments to compensate for the change in the moment of force.

2.2.3   Drag

Drag acts opposite and parallel to the velocity (Fig. 2-1b). The magnitude is constantly changing during flight but will never be zero. Drag is the main factor in slowing down the disc (gravity also slows the disc by affecting the vertical component of the velocity vector). To maximize the distance, the disc should be thrown at or near the angle of attack where drag is a minimum.

The drag magnitude is calculated as

$$D = \frac{1}{2}\rho v^2 A C_D \tag{2.2}$$

where $\frac{1}{2}\rho v^2$ is dynamic pressure, ρ is air density, A is planform area, v is relative velocity and C_D is the drag coefficient.

In general the drag coefficient is dependent on three quantities:

1) Reynolds number, Re

2) Spin parameter, S

3) Angle of attack, for asymmetrical bodies such as a wing or Frisbee.

Reynolds number is defined as the ratio of inertial forces to viscous forces

$$\text{Re} = \rho v d / \mu \tag{2.3}$$

where d is the diameter (or wing cord) and μ is dynamic viscosity of the fluid.

Potts and Crowther (2002) investigated drag and lift trends for $1.04 \times 10^5 < \text{Re} < 3.78 \times 10^5$ and found that the drag and lift coefficients are independent of Reynolds number. In addition, they have reported C_D for $\text{Re} = 3.78 \times 10^5$, equivalent to a flow speed of 20 m/s, for angles of attack from -10° to 30°.

Spin parameter is the ratio of the velocity of the outer edge due to spin to that due to translation

$$S = r\omega_z / v \tag{2.4}$$

where r is the radius and ω_z is the spin angular velocity. Spin will cause a small deflection in the wake of the flow but for Frisbees, Potts has shown spin rate to have a negligible effect on C_D.

Thus for a Frisbee, C_D (Fig. 2-2) is primarily a quadratic function of angle of attack as it is for lifting bodies in general (McCormick, 1995).

$$C_D = C_{D0} + C_{D\alpha}(\alpha - \alpha_0)^2 \tag{2.5}$$

There are two main components to the drag coefficient, the form drag C_{D0} and induced drag $C_{D\alpha}$. C_D never equals zero but there is a minimum drag, C_{D0}, which accounts for the skin friction and pressure drag. If not for induced drag, C_D would remain constant at C_{D0}. The drag in addition to C_{D0} is called induced drag, and can be shown to vary with lift as

approximately the square of C_L. Minimum drag occurs not at zero angle of attack but rather at the angle of attack where lift is zero. C_D is a minimum, $(C_D = C_{D0})$, when $\alpha = \alpha_0$, the angle of attack that produces minimum drag and zero lift. For most Frisbees, $\alpha_0 = -4°$.
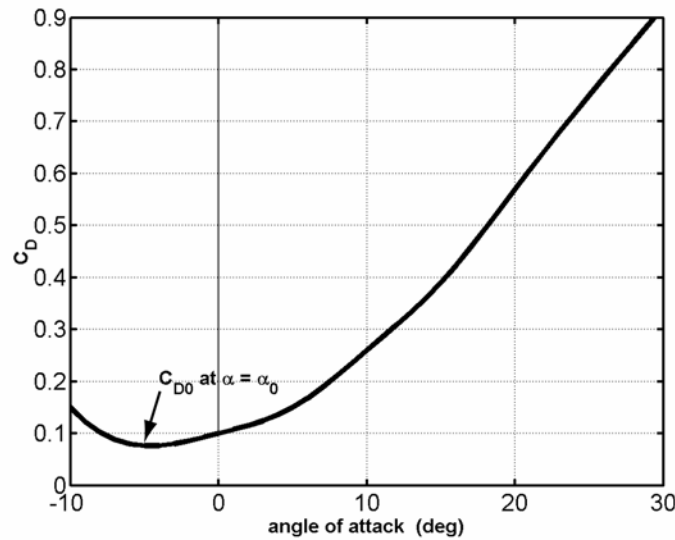
Figure 2-2 Drag coefficient C_D vs angle of attack, α.

2.2.4   Lift

Lift is defined to be perpendicular to the flow of the airstream (Fig. 2-1b). Lift will be directed roughly along the positive z axis for small angles of attack $\alpha > \alpha_0$ and along the negative z axis for $\alpha < \alpha_0$. Lift generally opposes the gravity, because the Frisbee plane and the velocity vector (initially) are both usually roughly horizontal. Balanced horizontal flight requires the lift magnitude to be equal to the gravity. During flight the airstream splits over the top and bottom at the disc's leading edge. When $\alpha=0$, the cambered shape of the Frisbee causes the horizontal incoming flow to be bent downward after leaving the trailing edge. When $\alpha > 0$, the front of the disc is tipped up, further deflecting the lower airstream downward. The upper airstream is also deflected downward. Known as the Kutta condition (Panton, 1995), fluids, including air, tend to adhere to and follow the

9

contour of a curved surface even when the surface bends away from the airstream. As the

Frisbee pushes down on the air, the air likewise pushes upward on the Frisbee in

accordance with Newton's third law which states for every force there is an equal and

opposite force. In this case, the force is known as lift. Lift also results due to suction.

Because of viscosity of the air, when the flow remains attached to the Frisbee the equal

and opposite forces cause a suction reaction from the airflow.

The combined effects of the cambered shape of the Frisbee and flight with positive angle

of attack, force the air flowing over the top to travel faster than the air flowing under,

producing a lower pressure region on the top than on the bottom. The increase in speed of

the upper airstream is accompanied by a substantial drop in air pressure above the

Frisbee. The change in pressure is accounted for by the Bernoulli equation. For horizontal

fluid flow, an increase in the velocity of flow will result in a decrease in pressure. The

integrated resulting pressure differential causes lift. Potts and Crowther (2002) collected

pressure data over the top and bottom for a non-spinning disc. Their results revealed the

incredibly complex nature of the pressure distribution on a Frisbee during flight.

Bernoulli's equation is useful for understanding the direction of the lift, but it is an

approximation for flows without vorticity. It is not a practical way to calculate the

magnitude of lift on a Frisbee, especially since the airflow and the pressure distribution

on the Frisbee are complicated by the Frisbee's asymmetric shape and spin.

The lift magnitude is calculated as

$$L = \frac{1}{2}\rho v^2 A C_L \tag{2.6}$$

similar to drag D (eq. 2.2) where here C_L is the lift coefficient.
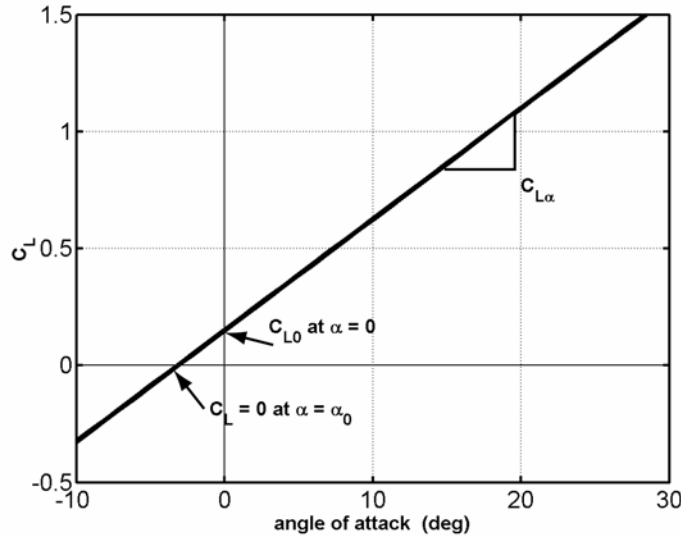
Figure 2-3 Lift coefficient C_L versus angle of attack, α

C_L (Fig. 2-3) can be approximated as a linear function of angle of attack, (McCormick, 1995) parameterized by two coefficients, the intercept C_{L0}, and the slope $C_{L\alpha}$.

$$C_L = C_{L0} + C_{L\alpha}\alpha \tag{2.7}$$

Note that when $\alpha = 0$, C_L is not zero, thus some lift is still generated due to the Frisbee's concave shape. As α increases, so does C_L and likewise the lift (until stall occurs at approximately $\alpha = 45°$). While drag cannot be zero, lift can. The angle of zero lift coincides with α_0, the angle of attack for minimum drag.

2.2.5 Aerodynamic Moments

The pressure and shear stress distribution cause a moment about the center of mass. Part of this moment is due to the lift and drag acting at the COP that does not coincide with

11

the COM (except when α=9° as shown in Fig. 2-4). This moment caused by the aerodynamic forces about the COM causes angular accelerations and precession. The location of the COP is primarily dependent on angle of attack. As the angle of attack changes throughout the flight, the COP moves and the magnitude of the moment will vary accordingly.

The components of the moments in the xyz axes of the Frisbee frame are called the roll R, pitch M, and spin down N moments, respectively (Fig. 2-1c) and are approximated by

Roll moment : $\qquad$ $R = \left(C_{R_r} r + C_{R_p} p\right)\frac{1}{2}\rho v^2 A d$ (2.8a)

Pitch moment : $\qquad$ $M = \left(C_{M_0} + C_{M_\alpha}\alpha + C_{M_q}q\right)\frac{1}{2}\rho v^2\, A d$ (2.8b)

Spin down moment : $N = \left(C_{N_r} r\right)\frac{1}{2}\rho v^2\, A d$ (2.8c)

Each moment is dependent on the dynamic pressure and area of the disc, as were lift and drag, but is additionally a function of the diameter of the disc and the angular velocity about the corresponding axis. Also, only the pitch moment is a function of α while roll and spin down are not. This is due to the way the moment axes were defined with x as the projection of the velocity vector on the disc plane.

The contribution to the moments has been identified, but what are their effects? As with lift and drag, each moment is composed of several aerodynamic coefficients which can be separated into three categories based on their effect (Table 2-1).

The spin down moment is proportional to a spin down coefficient, C_{N_r}, which accounts for the tendency of the disc spin rate about its axis of symmetry to decrease due to fluid

12

Table 2-1 Categories for aerodynamic moment coefficients.

Coefficient Category	Roll Moment	Pitch Moment	Spin Down Moment
Spin down			C_{N_r}
Wobble damping	C_{R_p}	C_{M_q}	
COP offset from COM	C_{R_r}	C_{M_0} and C_{M_α}	

viscosity. The roll and pitch moment each include a damping factor, C_{R_p} and C_{M_q} respectively, which result in the damping of the wobble. The last category contains the remaining three coefficients, C_{R_r} of the roll moment and C_{M_0} and C_{M_α} of the pitch moment. They are associated with the offset of the COP in the plane of the disc from the COM. C_{R_r} accounts for the roll moment due to spin, which results in a small pitch precessional angular velocity. The first two terms of the pitch moment M containing C_{M_0} and C_{M_α} are a function of α (Fig. 2-4) such that when $\alpha = 9°$, this component of the pitching moment
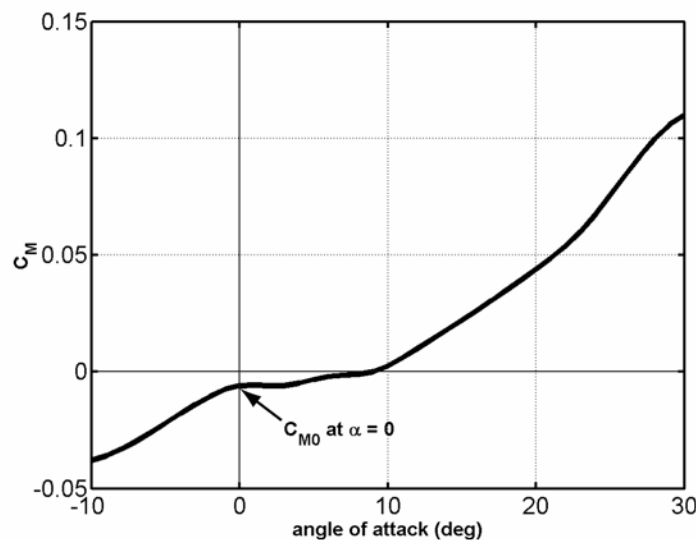
Figure 2-4 Pitch coefficient C_M versus angle of attack, α. $C_M=0$ at $\alpha=9°$ (Potts and Crowther, 2002).

will be zero. This angle of attack corresponds to front to back alignment of the COP with the COM. The specific values of the aerodynamic coefficients and their influence on flight are discussed in more detail in Chapter 3.

2.2.6   Miscellaneous Aerodynamics

As mentioned before, movement of the COP affects the direction and magnitude of the moments. The pitch moment varies as the COP moves forward and backward and as the component of the aerodynamic forces perpendicular to the disc plane changes. Both depend strongly on the angle of attack. A simple physical explanation for why the COP behaves as it does is not available in terms of fluid dynamic principles, but it relates to the shape of and flow around the Frisbee.

Often considerable influence on the aerodynamics of the Frisbee has been mistakenly attributed to the effect of the spin about the axis of symmetry. Consider the motion of the left and right sides of a Frisbee due to spin in a right hand backhand throw rotating clockwise viewed from above. The motion of the left side of the Frisbee (viewed from behind) is in the direction of the velocity while that of the right side opposes velocity. Consequently the total velocity on the left (due to spin and linear velocity of the COM) will be greater than that on the right. Since lift is quadratic in velocity (eq. 2.6), the distribution of the lift might consequently be thought to be greater on the left side than the right side. The COP would be expected to shift left of the midline of the disc to the side with the higher velocity. Such a shift would cause a positive roll moment.

However, data collected from Potts and Crowther (2002) shows the roll moment to be

negative, not positive. Thus the mistaken rationale presented above does not even

calculate the <u>sign</u> of the rolling moment, much less its magnitude, illustrating the

complex nature of the flow around the Frisbee. Also, it is important to understand that in

the lift calculation (eq. 2.6), C_L applies only to the Frisbee as a whole and the relative

velocity must be the velocity of the COM, not a left or right side velocity. In any case, the

roll moment is very small and does not play a large role in the flight dynamics.

As the Bernoulli equation predicts an upward force due to the increased flow velocity

over the top of the Frisbee, the differential velocity across the disc results in a side force

generated to the right. This side force is called the Robins-Magnus force. It is observed

in the curved trajectories of soccer balls and baseballs, where spin has been imparted.

However, for a Frisbee the resultant side force is near zero for low spin parameters,

S<0.35 (Potts and Crowther, 2002) and has been neglected in the equations of motion.

2.2.7   Concentric Rings

The Frisbee design includes an approximately 9.5 cm inner radius to 11.5 cm outer radius

region of concentric surface roughness rings on the top sloping surface (not on the top

flat plane of the Frisbee). The purpose of these rings is to manipulate the boundary layer

and ultimately reduce drag. The boundary layer is a region of relative motion between

adjacent layers of fluid particles. There is a no-slip condition between the air and the

Frisbee at its surface, but moving away from the Frisbee the velocity profile changes until

the velocity of the airflow in the boundary layer matches the airflow unaffected by the motion of the Frisbee.

Theoretically, as the air moves across the concentric rings, flow in the boundary layer transitions from laminar to turbulent flow. By virtue of the increased energy in the boundary layer, the air flow stays attached to the surface of the Frisbee longer, delaying separation more than if the flow were laminar. Drag is minimized by keeping the airflow connected to the surface as long as possible. The significance of the rings' influence is debatable though a well worn disc with many dings and scratches will produce different flight characteristics compared to an identical but new disc.

2.3   Gyroscope

How does spin affect the flight? Spin has been shown to have little affect on the aerodynamics of a Frisbee but it does have a critical role in the flight dynamics. Although the lift and drag coefficients are unaffected by spin and the pitch and roll moments are affected but only by a very small amount (Potts and Crowther, 2002), the critical aspect of the spin is the stability it provides in flight due to angular momentum and gyroscopic precession.

2.3.1   Angular Momentum

Angular momentum, $\mathbf{H}$, is the product of the spin angular velocity vector of the Frisbee in inertial space, $\boldsymbol{\omega}$, and the inertia matrix, $\mathbf{I}$

$$\mathbf{H} = \mathbf{I}\boldsymbol{\omega} \tag{2.9}$$

These vector/matrix quantities are usually expressed in the reference frame F since

angular momentum is easily calculated in this frame because $\mathbf{I}$ is constant in the principal

axes and $I_{xx} = I_{yy}$ due to symmetry. Note that even though the frame F is not fixed in the

Frisbee, the axes of F are nevertheless principal axes.

Table 2-2 Moments of inertia for a Frisbee (experimentally determined) and a flat disc of
equal mass.

	Frisbee (kg-m²)	Flat Disc (kg-m²)	Difference
I_{zz}	0.00235	0.0016	47 %
I_{xx}, I_{yy}	0.00122	0.0008	53 %

The Frisbee has relatively high axial and transverse moments of inertia compared to a flat

disc of equal mass and diameter (Table 2-2) because a large portion of the disc's mass is

on the bulky rim increasing the average distance squared of the mass from the axis of

rotation ($I=mr^2$). Since the inertia does not change, the only variable is spin. Thus by

spinning the disc faster, angular momentum is increased.

From Euler's expression of the principle of rate of change of angular momentum,

$$^{N}\dot{\mathbf{H}} = \mathbf{M} \tag{2.10}$$

where $^{N}\dot{\mathbf{H}}$ is the rate of change of the angular momentum with respect to an inertial

reference frame, N, and $\mathbf{M}$ is the sum of all moments acting on the Frisbee. Since $\mathbf{H}$ is

expressed in the F frame, the derivative of $\mathbf{H}$ in the inertial frame is given by (Meriam

and Kraige, 1992)

$$^{N}\dot{\mathbf{H}} = {}^{F}\dot{\mathbf{H}} + {}^{N}\boldsymbol{\omega}^{F} \times \mathbf{H} \tag{2.11}$$

where the derivative of $\mathbf{H}$ in the F frame is given by $^{F}\dot{\mathbf{H}} = \mathbf{I}\dot{\boldsymbol{\omega}}$, $^{N}\boldsymbol{\omega}^{F}$ is the angular

velocity of the F frame in the inertial frame, and the $^{N}\boldsymbol{\omega}^{F} \times \mathbf{H}$ term is the difference

between the derivatives of **H** in the F and N frames. This last term describes the

precession of the Frisbee.

The law of conservation of angular momentum states that the angular momentum of an

object remains constant as long as no external torques, or moments, act on that object,

$^{N}\dot{\mathbf{H}} = \mathbf{M} = 0$. This means that a spinning disc without any external moments will

maintain a constant angular momentum direction and magnitude in inertial space. When

a moment does act on the object, $^{N}\dot{\mathbf{H}} = \mathbf{M} \neq 0$, the moment produces (causes) a rate of

change of **H**, which can result in a rate of change in both the magnitude and the

orientation of the **H** vector. Precession is change in the orientation of the angular

momentum vector of constant magnitude, observed when the axis of spin turns about

another axis. The angular momentum helps to resist the effects of the moments. In other

words, increasing angular momentum by increasing spin decreases the precession rate

caused by moments perpendicular to **H**. This relationship is discussed in more detail

later.

2.3.2   Wobble

The wobble observed during the flight of the Frisbee is due to two main effects. First, the

Frisbee will wobble if there are any components of angular velocity about the x and y

axes. These angular velocities may be induced at release. Learning to throw the Frisbee

wobble free (i.e. without initiating these angular velocities) results with practice. The

second source of wobble results from the aerodynamic moments acting on the disc.

The effects of both sources of wobble are illustrated first by neglecting the aerodynamic moments. Because the xyz axes are principal axes, the Euler equations expressing $\dot{\mathbf{H}} = \mathbf{M}$ when $\mathbf{M} = 0$ are

$$\sum M_x = I_{xx}\dot{\omega}_x - \left(I_{yy} - I_{zz}\right)\omega_y\omega_z = 0 \tag{2.12a}$$

$$\sum M_y = I_{yy}\dot{\omega}_y - \left(I_{zz} - I_{xx}\right)\omega_z\omega_x = 0 \tag{2.12b}$$

$$\sum M_z = I_{zz}\dot{\omega}_z - \left(I_{xx} - I_{yy}\right)\omega_x\omega_y = 0 \tag{2.12c}$$

(ω_x, ω_y, and ω_z refer to the angular velocities p, q, and r respectively about the xyz axis, as shown in Fig. 2-1c, likewise $\dot{\omega}_x, \dot{\omega}_y$, and $\dot{\omega}_z$ are equivalent to $\dot{p}, \dot{q}$, and $\dot{r}$ respectively.)

Since $I_{xx} = I_{yy}$, the third Euler equation (2-12c) shows that $\dot{\omega}_z = 0$ and thus the spin ω_z is constant. Further, equations 2-12a and 2-12b can be linearized about the constant spin ω_z to show that the disc wobbles at a frequency of twice the spin frequency. That is ω_x and ω_y oscillate sinusoidally at roughly twice the frequency ω_z. Hence, in torque free motion, the axial spin will be constant and the plane of the Frisbee will wobble continuously.

At the beginning of most throws, particularly beginner throws, a wobble is noticeable. Fortunately, this wobble quickly dies out because the Frisbee is not an example of torque free motion. Rather moments on the Frisbee cause the angular velocities to change, and essentially act to dampen out the wobble and induce precession.

The gravity does not affect angular momentum because it acts through the COM and does not generate a torque on the disc. However the COP is offset from the COM (Fig. 2-1a) so the aerodynamic forces do exert a torque on the Frisbee. To illustrate how the torque causes precession, consider the lift generated during a flight when the angle of attack is

less than 9°. For this condition, the lift acts behind the COM producing a negative

pitching moment, pointed to the "left". If there were no angular momentum, the Frisbee

would angularly accelerate about the pitch axis causing the front of the Frisbee to rotate

nose down. However this clearly does not happen when the disc is thrown with

substantial spin. Rather, for $\alpha < 9°$, the Frisbee will roll to the right. This occurs because

the change in the angular momentum is equal to the moment, $\dot{\mathbf{H}} = \mathbf{M}$, meaning that the

angular momentum vector must rotate towards the direction of the moment (Fig. 2-5). In

this case, the moment is pointed to the left, so $\dot{\mathbf{H}}$ is to the left, and as the angular

momentum vector rotates to the left, the left side of the Frisbee will rotate up causing the
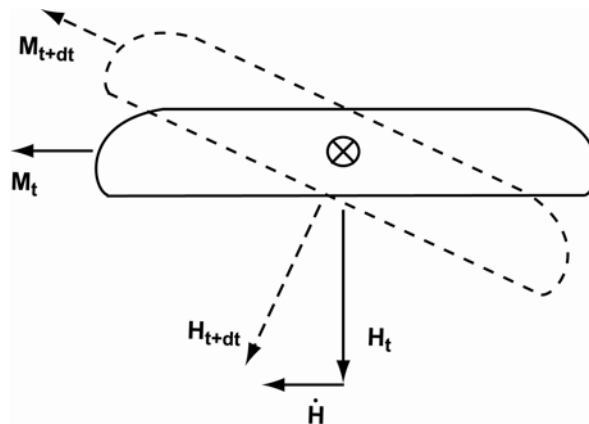
Figure 2-5 Angular momentum vector **H**, at some initial time, t, and a later time, t+dt due
to the rate of change of **H**. View from back of Frisbee with the velocity vector into the
page, and a negative pitch moment directed to the left.

Frisbee to roll to the right. Thus a negative pitching moment will cause the disc to roll

right while a positive pitching moment will cause the disc to roll left. Likewise, a

negative roll moment (vector points back) will cause the front of the disc to nose down,

while a positive roll moment will cause the Frisbee to pitch up. In general, a pitching

moment causes precessional roll rate and a roll moment causes a precessional pitch rate.

This important aspect of the spin is critical to understanding the dynamics of stable flight.

Previously it was mentioned that an increase in **H**, specifically the magnitude of the axial component, H_z, will reduce the effects of precession. Remember that H_z is a linear function of the spin rate ω_z, $H_z = I_{zz}\omega_z$, where I_{zz} is the moment of inertia about the spin axis. This spin rate and the rate of precession $\dot{\Psi}$, are directly related. Because the precession rate of the constant magnitude H_z is $\dot{\Psi}$, the rate of change of H equals $\dot{\Psi}H = I_{zz}\dot{\Psi}\omega_z$. Because $\dot{\mathbf{H}} = \mathbf{M}$ then

$$M = I_{zz}\dot{\Psi}\omega_z \tag{2.13}$$

For a given moment and constant I_{zz}, if the spin rate ω_z is increased, then the precessional rate $\dot{\Psi}$ will decrease.

2.4 Investigation of flight trajectories

The aerodynamic forces and moments are constantly changing throughout the flight. Armed with the mechanisms operating during Frisbee flight, trajectories often observed can be analyzed and explained. The Frisbee can be thrown such that straight nearly horizontal flight is possible over a long distance, up to 20 m or more. Frisbees also have the ability to curve left or right during certain portions of the flight. What are the flight conditions that result in such trajectories?

2.4.1   Analysis of horizontal straight flight

There are no real life conditions that will produce a perfectly horizontal straight flight, but a close approximation to this trajectory can be made. Analysis of this type of flight is useful for interpreting the relationship between angle of attack and velocity. To

21

approximate these flight conditions, the rolling and pitching moments are assumed to be zero, preventing wobble and precession. Thus the orientation of the disc will remain unchanged during flight. In addition, for the flight to be horizontal the lift must equal the weight at all times. Recall from eq. 2-6 that lift is quadratic in velocity and also dependent on angle of attack. The velocity (eq. 2-14) required to produce lift equal to the gravity thus can be calculated for any angle of attack.

$$mg = L = \frac{1}{2}\rho v^2 A C_L$$

Solving for v and substituting $C_L = C_{L0} + C_{L\alpha}\alpha$

$$v = \sqrt{\frac{2mg}{\rho A(C_{L0} + C_{L\alpha}\alpha)}} \qquad (2.14)$$

Figure 2-6 illustrates the relationship between the two variables in eq. 2-14, angle of attack and velocity. For the lift to equal the gravity, as the velocity decreases the angle of
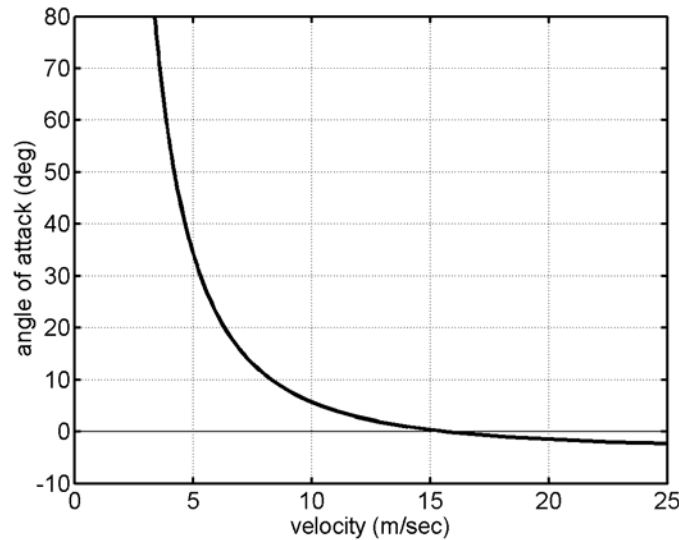
Figure 2-6 Velocity and angle of attack relationship for lift to balance weight.

22

attack must increase. For example, when α = 0 the Frisbee must be thrown at 16 m/s to produce horizontal flight. Drag will inevitably cause the Frisbee to slow down. Accordingly the lift will decrease, and once it is less than gravity the Frisbee would then start to fall. Since the orientation of the disc does not change (since moments are assumed to be zero), the angle of attack increases as the direction of the velocity vector points down. Lift increases with an increase in angle of attack (Fig. 2-3) providing the extra lift needed to balance the weight when the velocity decreases. Long sustained nearly level flights are possible because as the Frisbee slows down, lift can be maintained at a magnitude nearly equal to the weight.

2.4.2 Downward steady gliding

The above is an approximation because the flight will be straight only when the rolling and pitching moments are equal to zero which occurs only when α=9°. As shown above, however, as the velocity decreases the angle of attack must increase, producing a pitching moment. However a straight trajectory is possible during a steady downward glide.
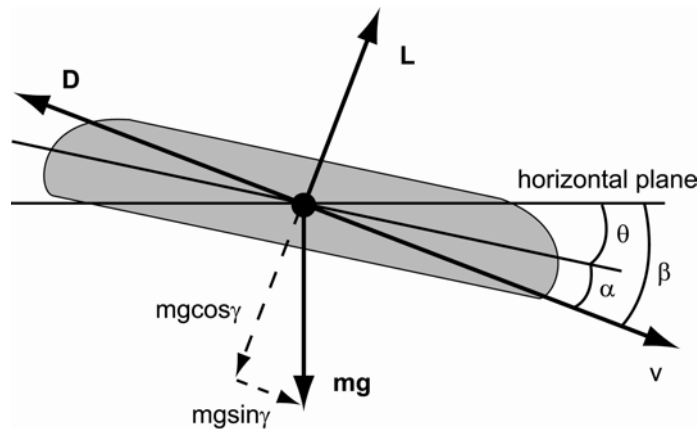
Figure 2-7 Force balance for steady downward gliding, α=9°, θ=-10.3°, β=-19.3°, COM=COP.

The pitching and rolling moments still need to be zero, but now they can be approximately maintained. To first achieve zero pitching and rolling moments, the Frisbee must be thrown with no initial wobble, i.e. without any angular velocity components about the x and y axes that would cause pitch and roll rates (p and q) and corresponding moments in eq. 2-8. Secondly, the angle of attack must be $\alpha = 9°$. At this angle, the remaining terms of the pitching moment will be zero (Fig. 2-4).

Previously there was nothing to balance the drag, but with the orientation of the Frisbee nose down with the velocity vector pointed below the plane of the Frisbee, there is now a component of the weight to balance drag. Together the lift and drag can balance the weight (Fig. 2-7) for a given velocity and given downward glide angle, β, the angle between the velocity vector and the horizontal.

$$mg\cos\beta = \mathbf{L} = \frac{1}{2}\rho v^2 A C_L \qquad (2.15a)$$

$$mg\sin\beta = \mathbf{D} = \frac{1}{2}\rho v^2 A C_D \qquad (2.15b)$$

Solving the above two equations simultaneously gives

$$\beta = \tan^{-1}\left(\frac{C_D}{C_L}\right), \text{ where } \beta = \alpha + \theta \qquad (2.16)$$

for $\alpha = 9°$, $\beta = -19.3°$, and $C_D = .024$ and $C_L = 0.67$ as specified by Figs. 2-2 and 2-3 respectively. At this orientation the angle between the horizontal and Frisbee plane is $\theta = -10.3°$, the Frisbee will not precess and it can fly straight at $v = 9.1$ m/s.

2.4.3   Common Throw Conditions

Common release conditions for a 25 m flight performed by an experienced thrower with little initial wobble are velocity $v = 14$ m/s, spin r = 50 rad/sec, pitch angle $\theta = 11°$, roll

angle φ= 0° and angle of attack α =5° (Fig. 2-8). A simulation of a flight using these

conditions was performed to investigate the trajectory. Immediately the Frisbee starts to

curve right (Fig. 2-9a). This occurs when the angle of attack is less than 9° (Fig. 2-9b),

during which the Frisbee will have a negative pitch moment causing the Frisbee to roll

right. Remember, if the spin is high this tendency to roll right will be less than if the spin

is lower. Initially the velocity vector is pointed slightly above horizontal and the lift is

sufficiently large to overcome the weight causing the Frisbee to accelerate upward.

Because drag and gravity slows the disc down, by the end of the flight the velocity has

decreased to nearly 1/3 its original speed to less than 4 m/sec. Decreasing speed means
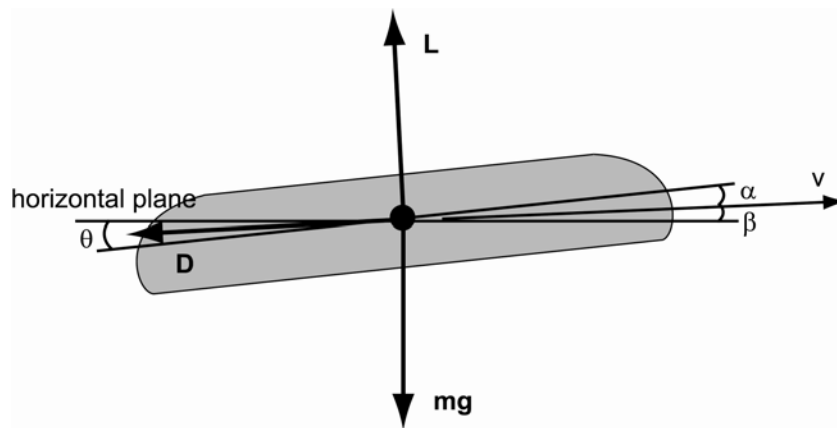
Figure 2-8 Force and flight configuration for α=5°, θ=11, β=6°.

the lift will no longer exceed weight and the Frisbee will start to fall. However, as the

downward component of velocity increases, the angle of attack increases. Lift increases

with increased angle of attack; therefore the Frisbee does not fall as fast as it would if the

angle of attack remained constant. Because the pitch angle does not change much, less
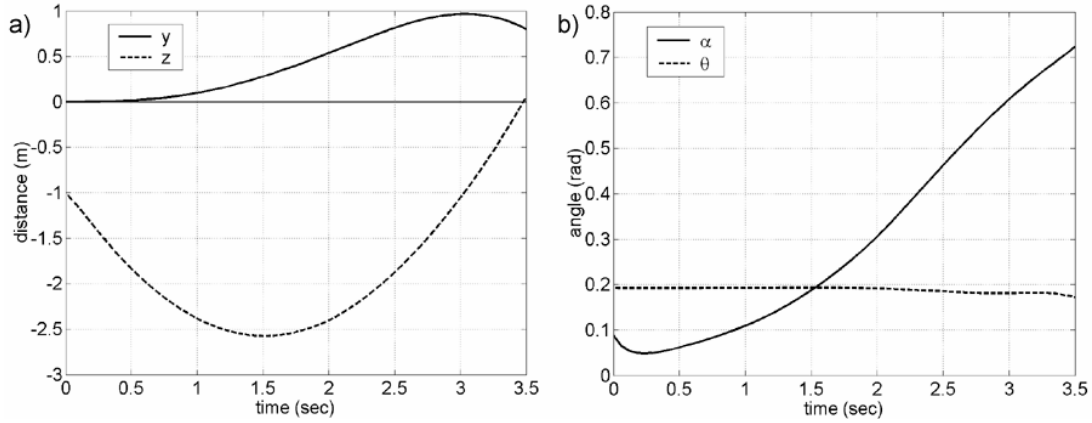
Figure 2-9 Simulation results of a 25 m flight with release conditions $v = 14$ m/s, $r = 50$ rad/sec, $\alpha = 5°$, $\varphi = 0°$, and $\theta = 11°$.

a) y and z components of the COM displacement. Immediately the Frisbee starts to curve to right (increasing Y), after three sec the Frisbee curves back to the left (decreasing Y). Initially the Frisbee is released 1 m high and it reaches a maximum height of 2.55 m before hitting the ground at 3.5 sec.

b) Angle of attack α and pitch angle θ. α starts at 6° and remains below 9° (0.157 rad) for the first 1.25 sec, then increases till the end of the flight. θ remains fairly constant changing less than 2° (0.035 rad) throughout the flight. Since the pitch orientation does not change much but the angle of attack does, the Frisbee must be falling (velocity vector points below horizontal).

than 2° (Fig. 2-9b), angle of attack will continue to increase as long as the Frisbee is

slowing down and falling. Also, once the angle of attack exceeds 9°, the pitching moment

becomes positive (the COP moves forward of the COM) which results in a negative roll

rate and the right side of the Frisbee (viewed from the back) to rotate up, causing the

common "left curve" of the disc at the end of a flight (Fig. 2-9a). The time histories of all

the states for the flight are shown in Fig. 2-10. The magnitudes of the forces and

moments for the simulation are shown in Fig. 2-11.

26
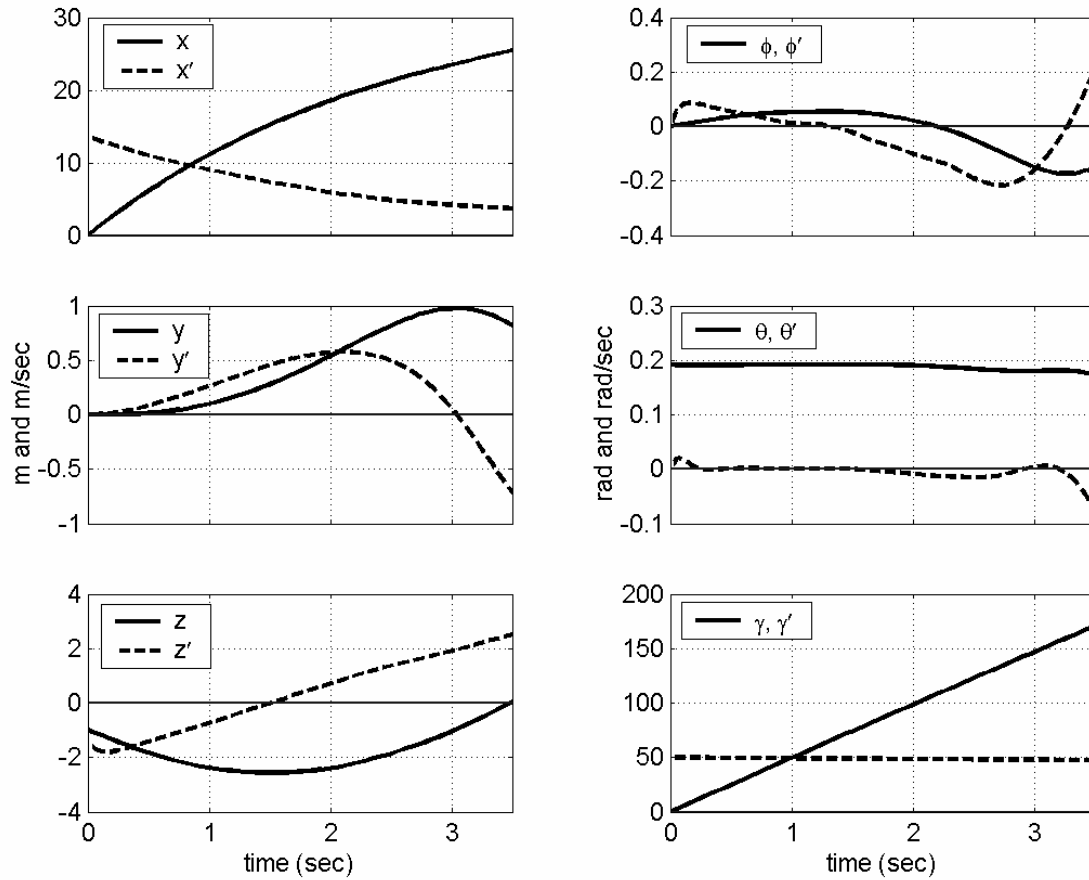
Figure 2-10 All states, position, orientation and their derivatives, for a simulation of a 25 m flight with release conditions of v = 14 m/s, r = 50 rad/sec, α = 5°, φ = 0°, and θ = 11°. position/orientation angle (solid line) velocity/angular velocity (dashed line).

2.5 Lure of the Frisbee

One train of thought is that the perfect Frisbee is a design in which the COP always coincides with the COM, preventing torque formation and precession, thus allowing for anyone to easily throw the Frisbee straight. The shape of the Frisbee can be designed to position the COP with the COM for a specified angle of attack. Doing this for the broad ranges of angles of attack a Frisbee experiences during flight presents many challenges.
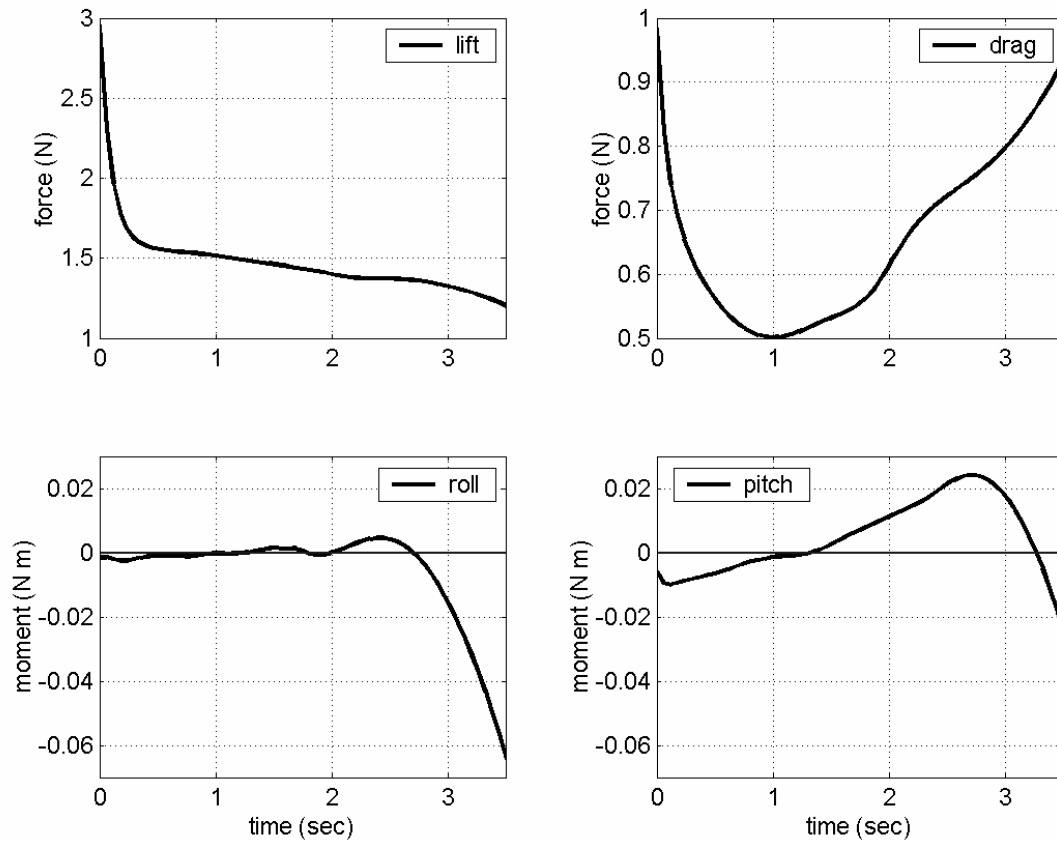
Figure 2-11 All forces and moments, for a simulation of a 25 m flight with release conditions of v = 14 m/s, r = 50 rad/sec, α = 5°, φ = 0°, and θ = 11°.

These efforts may not be worthwhile. By altering the release conditions of a throw, the torques generated during flight can be directed by the practiced thrower to produce a straight trajectory. But more importantly, they also can be manipulated to create throws with beautifully curved flights of boundless variety. This ability is what separates the Frisbee from other flying sports implements. This ability is the lure of the Frisbee.

28

Chapter 3   Identification of Frisbee Aerodynamic Coefficients Using Flight Data

3.1   Abstract

An alternate method to wind tunnel tests for the identification of aerodynamic coefficients of the Frisbee is presented. The method is based on matching actual flight data with predicted data from a simulation model. Three reflective markers or active LEDs are placed in a triangular array on the upper surface of the disc. Their positions during actual flights are tracked in three dimensions using high-speed video cameras. The Newton-Euler flight simulation model includes 10 aerodynamic coefficients relating linear approximations of aerodynamic forces and moments to the disc angle of attack and to its linear and angular velocities. Parameters (including coefficients and flight initial conditions) are estimated with an optimization algorithm that iteratively modifies the parameters to minimize the differences between predicted and estimated marker positions. Good estimator performance depends heavily on accurate measured data and on the set of flights spanning a wide range of angles of attack. Predicted aerodynamic coefficients compare reasonably well with linearized approximations of wind tunnel results from the literature.

3.2 **Introduction**

More flying discs are sold each year than baseballs, basketballs, and footballs combined, but until recently scientific research on its flight mechanics was relatively scarce. Stilley (1972) investigated a self-suspended Frisbee-like flare and used wind tunnel studies to measure the aerodynamic lift and drag on the Frisbee as a function of angle of attack, α, the angle between the velocity vector and the Frisbee plane. Spinning and non-spinning wind tunnel tests showed that the effect of spin on aerodynamic forces and moments is small. Stilley & Carstens (1972) analyzed flight stability and compared actual flights to free-fall tests. Mitchell (1999) also measured Frisbee lift and drag using wind tunnel tests. He confirmed the observation of Stilley that spin affects lift and drag only little. Yasada (1999) measured lift and drag over a range of speeds and spin rates for a Frisbee shaped disc and a flat disc.

Recently Potts and Crowther (2000; 2001; 2002) studied the aerodynamics in an exhaustive series of wind tunnel tests. They accurately measured lift and drag and pitching and rolling moment as a function of Reynolds number and spin parameter, the ratio of speed at the edge of the disc due to spin to the speed of the center. They corroborated the results of Stilley and Carstens (1972) at zero spin. Slight differences in lift and pitching moment were attributed to the different cross sectional shapes and thickness ratios of the Frisbees tested from those of Stilley and Carstens. Potts and Crowther found little effect of Reynolds number on lift and drag except at high angles of attack ($\alpha \geq 20°$). Although they detected virtually no effect of spin parameter on lift and drag, non-zero rolling moments

and small but distinct effects of spin parameter on pitching and rolling moments were observed.

Lissaman (1993) investigated the flight stability of an oblate spheroid by considering the effect of each stability derivative (aerodynamic coefficient) on the characteristic equation.

In related work, Soong (1976) analyzed the dynamics of the discus throw, whose shape differs from that of the Frisbee mainly in that it has a plane as well as an axis of symmetry. Soong did not include any rolling aerodynamic moments and showed that the main effect of pitching moment is to cause a precession of the spin in roll, thus decreasing lift later in the flight.

Frohlich (1981) also investigated the flight dynamics of the discus. With computer simulations that relied on discus lift and drag coefficients determined experimentally by Ganslen (1964) and others, he showed that the discus can be thrown farther against the wind than with it. Although this paper included a complete discussion of the qualitative effects of aerodynamic moments on the subsequent flight, the analysis remains somewhat hypothetical because of the absence of any experimental data on pitching and rolling aerodynamic moments. Frohlich also noted the remarkable similarity between the discus and the Frisbee.

Simulation of the motion of a complete Frisbee flight requires knowledge not only of initial conditions, but also of the dependence of all forces and moments experienced by

the Frisbee on its dynamic motion through the air. As an alternative to time-consuming wind tunnel tests to measure these forces and moments, often analytic piecewise linear approximations are used for the functional dependence of the forces and moments on their arguments. The constants relating the linear approximations of these forces and moments to angles, velocities and angular velocities are called aerodynamic coefficients or stability derivatives. Such coefficients play a central role in stability investigations (Lissaman, 1993), but are also a simpler alternative to the use of "look-up" tables of measured force and moment data in the integration of the flight equations to predict Frisbee flight dynamics.

This paper contains a description of the implementation of a scheme for the estimation of aerodynamic coefficients for the Frisbee. The algorithm is essentially an informed search in parameter space for the set of parameters that minimizes a performance index consisting of the mean squared difference between trajectories measured in actual flights and those predicted using the parameters in a simulation.

3.3   Methods

3.3.1   Simulation Model

Since the Frisbee is a rigid body, the differential equations describing flight are similar to those for aircraft (Etkin and Reid, 1996). These are typically a Newton-Euler formulation relating the rates of change of linear and angular momenta to the forces and moments experienced from gravity and aerodynamics, and are usually expressed in body fixed coordinates. A body-fixed reference frame is achieved from an inertial frame using 1-2-3

rotations of ϕ, θ and γ which specify the general orientation of the disc. Because the Frisbee is axially symmetric, it is possible to coordinatize the equations of motion in a frame associated with the velocity vector, rather than in a body-fixed frame.

Figure 3-1 shows a schematic of the Frisbee in flight. The coordinate axis x_F lies along the projection of the velocity vector on the Frisbee plane. The z_F axis of symmetry is perpendicular to the Frisbee plane and points generally downward, and y_F is the cross product of z_F and x_F. The equations of motion, the details of which are summarized in the
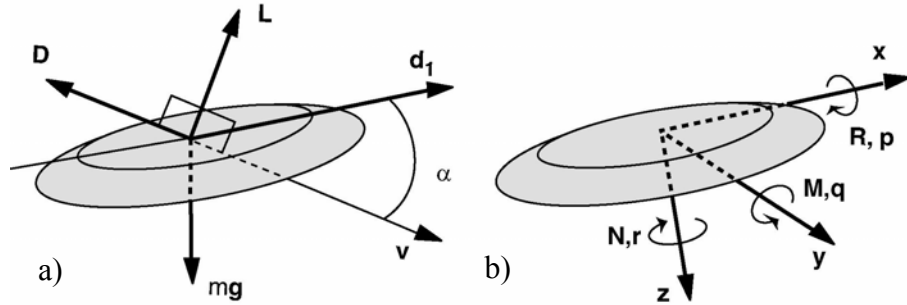
Figure 3-1 a) Drag **D** and lift **L** act in a plane perpendicular to the disc plane and opposite and perpendicular to the velocity **v,** respectively**.** They are primarily functions of the angle of attack, α, the angle between **v** and $\mathbf{d_1}$ in the disc plane. b) xyz axes of the disc; roll **R**, pitch **M** and spin down **N** moments; roll p, pitch q and yaw r angular velocities.

appendix, are a Newton-Euler description of the motion of a rigid body. These are expressed in the reference frame F since, because of symmetry, F is a set of principal axes of inertia for the disc. The equations of motion in schematic form are

$$m\left(\frac{d\mathbf{v}}{dt} + \omega_F \times \mathbf{v}\right) = \mathbf{F} \text{ - } \mathbf{mg} \tag{3.1}$$

$$I\frac{d\omega}{dt} + \omega_F \times I\omega = \mathbf{M} \tag{3.2}$$

where $\omega = \dot{\varphi}\cos\theta\mathbf{x_F} + \dot{\theta}\mathbf{y_F} + (\dot{\varphi}\sin\theta + \dot{\gamma})\mathbf{z_F}$ and is the inertial angular velocity of the body, m is the mass, g is gravitational acceleration, I is the mass moment of inertia matrix, ω_F is the angular velocity of the coordinate frame, and the resultant vectors of aerodynamic force and moment $\mathbf{F}$ and $\mathbf{M}$ are due to aerodynamics alone (Hubbard and Hummel, 2000). The two contributors to $\mathbf{F}$, the lift $\mathbf{L}$ and drag $\mathbf{D}$, act perpendicular and opposite to the velocity vector $\mathbf{v}$, respectively, and are strong functions of the angle of attack, α, the angle (Fig. 3-1) between $\mathbf{v}$ and $\mathbf{d_1}$ where $\mathbf{d_1}$ is equivalent to x_F. A steadily spinning body ω experiences a Robins-Magnus side force perpendicular to the plane determined by the velocity and angular velocity vectors. Although this force has been measured by Potts, it is small and is neglected here. The only other force acting is gravity.

The Frisbee flight model presented here contains ten coefficients, denoted below by the symbol C_{Ij}. In each case the coefficient has two subscripts. The first I denotes the dependent variable (force or moment) being approximated, and the second j denotes the major independent variable on which the force or moment is assumed to depend. Thus each coefficient (except for C_{Lo} and C_{Do} which are constants and $C_{D\alpha}$, in which the dependence on α is quadratic) is a partial derivative of a force or moment with respect to an angle or angular velocity. To a first approximation, lift and drag are linear and quadratic functions, respectively, of the angle of attack (Anderson, 2001). The complete model for the aerodynamic forces and moments is

$$\text{Lift}: \quad L = \left(C_{L0} + C_{L\alpha}\alpha\right)\frac{1}{2}\rho v^2 A \tag{3.3}$$

$$\text{Drag}: \quad D = \left(C_{D0} + C_{D\alpha}(\alpha - \alpha_0)^2\right)\frac{1}{2}\rho v^2 A \tag{3.4}$$

$$\text{Roll moment}: \quad R = \left(C_{R_r}r + C_{R_p}p\right)\frac{1}{2}\rho v^2 Ad \tag{3.5}$$

$$\text{Pitch moment}: \quad M = \left(C_{M_0} + C_{M_\alpha}\alpha + C_{M_q}q\right)\frac{1}{2}\rho v^2\, Ad \tag{3.6}$$

$$\text{Spin down moment}: \quad N = \left(C_{N_r}r\right)\frac{1}{2}\rho v^2\, Ad \tag{3.7}$$

$$\tag{3.8}$$

where L and D are the lift and drag; R, M, and N and p, q, and r are the roll, pitch and yaw

moments and angular velocities, respectively, in the x_F, y_F, z_F frame (Fig. 3-1); A and d are

the Frisbee planform area and diameter, respectively; ρ the atmospheric density, v is the

speed, and α_0 is the angle of attack at zero lift and minimum drag (Table 3-1).

Table 3-1 Values of non-aerodynamic simulation parameters

Parameter	m	I_{zz}	I_{xx}, I_{yy}	d	A	ρ	g
units	kg	kg-m^2	kg-m^2	m	m^2	kg/m^3	m/s^2
	0.175	0.00235	0.00122	0.269	0.057	1.23	9.794

The determination of these coefficients is the subject of the remainder of the paper. Given

values for the ten coefficients, integration of the differential equations of motion yields the

motion dynamics. Furthermore, using the time histories of the six rigid body configuration

variables (including both center of mass positions and angular orientations), and the

known positions of three reflective markers on the Frisbee surface (see description below),

it is possible to calculate the predicted inertial xyz coordinates of the markers as functions

of time. As the Frisbee translates and rotates the markers follow a sinusoidal path through

space. The comparison of these predicted marker trajectories to those determined

experimentally in actual flights is the basis of the estimation scheme for the determination

of the aerodynamic coefficients.

3.3.2   Experimental flight data

Two separate experiments were performed to collect in-flight data. The first experiment

(short flights) tested atypical Frisbee throws, i.e. velocity $v = 3$ m/sec, spin r = 8.91

rad/sec and the flight distance x = 2 m. A second experiment (long flights) measured

typical throws, (velocity $v = 14$ m/sec, spin r = 50 rad/sec and the flight distance x = 18

m). Four high speed (120 Hz for short flights, 200 Hz for long flights) video kinematic

data acquisition cameras and standard DLT techniques were used to record the xyz

locations of the three markers on the Frisbee during multiple flights. In initial short flights,

three reflective tape markers were placed on the top Frisbee surface. Reflectivity of the

markers is a strong function of the angle of incidence from the surface normal direction.

Thus tracking of the markers proved difficult in later experiments with the longer flights

and reflective markers were replaced by active light emitting diodes (LEDs) in a similar

triangular configuration on the Frisbee upper surface. The four cameras captured the entire

short flight experiments, however in the long flights experiment, only the beginning and

ending 2-3 m were collected. The short flight position data, with the dynamic flight model

(Hubbard and Hummel, 2000), allows the estimation of the aerodynamic force and

moment coefficients using an iterative estimation algorithm. For the long flights data, the

estimation algorithm was replaced by a MATLAB optimization function. Rather than

optimize for all 10 aerodynamic coefficients, this function optimized for the three angular

velocity dependent coefficients not previously determined in wind tunnel testing, C_{Mq}, C_{Rp}, and C_{Nr}.

3.3.3 Parameter estimation algorithm

A MATLAB computer program for the short flights data was written implementing the following steps:

1. Guess 12 initial conditions (for six rigid body degrees of freedom and six associated velocities) for each of n experimental flights and values for the 10 coefficients. This results in a total of 10+12n unknown parameters to be estimated. The vector of parameters is denoted by **p,** and n corresponds to the number of flights run in the estimation algorithm at one time.

2. Simulate (integrate the ODE's for) each flight given the parameter vector **p**.

3. Use the simulated state variables to predict the xyz motion of the markers.

4. Calculate the residual, defined as the sum of squared differences between the predicted and measured xyz marker motions for all times over all flights.

5. Using 10+12n other simulations calculate both the gradient and approximate Hessian of the residual with respect to **p**.

6. Determine a correction to the parameters **p** (both initial conditions and coefficients) that reduces the residual using the method described by Hubbard and Alaways (1989).

7. Return to step 2 until the residual is below a minimum value.

It was necessary to use data from several (n=3) flights containing trajectory information over a wide range of α to yield accurate coefficient estimates.

3.3.4 Parameter Optimization

A MATLAB computer program for the long flights data was written implementing the following steps:

1. Guess 12 initial conditions (for six rigid body degrees of freedom and six associated velocities) for a given experimental flight and values for the three coefficients, C_{Mq}, C_{Rp}, and CNr. This results in a total of 3+12 unknown parameters to be optimized. The vector of parameters is denoted by **p**.

2. Call MATLAB function *fminsearch* which will simulate (integrate the ODE's for) each flight given the parameter vector **p**.

3. Determine a correction to the parameters **p** (both initial conditions and coefficients) that reduces the residual, defined as the sum of squared differences between the predicted and measured xyz marker motions for all times over all flights, according to *fminsearch* guidelines specified in MATLAB.

The other seven aerodynamic coefficients were not optimized in this method because they are strongly dependent on angle of attack. The long flights data all contained flights where angle of attack varied less than 10°. Instead, the seven coefficients were specified according to the values reported by Potts and Crowther (2002).

3.4 Results

The results of the aerodynamic coefficients, found from the short flights and long flights experiments are summarized and compared to linear approximations of the lift, drag and pitching moment measured by Potts and Crowther (2002), Yasada (1999), and Stilley and

Carstens (1972) (Table 3-2). Other than the results listed from this research, the right hand side of the table is vacant, except for one measurement made by Potts and Crowther. The final four coefficients in Table 3-2 correspond to the dependence of pitching, rolling and yawing moments on the three components of angular velocity. Because generally wind tunnel tests to determine angular velocity dependent coefficients are extremely difficult if not impossible to perform, parameter estimation provides an attractive alternative. Wind tunnel measurement techniques cannot measure a moment about an axis that is spinning. This technique in this paper using parameter estimation is an effective method for obtaining estimates of the three damping coefficients C_{Mq}, C_{Rp} and C_{Nr}.

Table 3-2 Comparison of aerodynamic coefficients to linear approximations of measured values from Potts and Crowther (P&C), Yasada, and Stilley and Carstens(S&C).

	C_{Lo}	$C_{L\alpha}$	C_{Do}	$C_{D\alpha}$	C_{Mo}	$C_{M\alpha}$	C_{Mq}	C_{Rr}	C_{Rp}	C_{Nr}
short flights	0.33	1.91	0.18	0.69	-0.08	0.43	-5.0E-3	1.4E-2	-5.5E-3	-7.1E-6
long flights	---	---	---	---	---	---	-1.4E-2	---	-1.3E-2	-3.4E-5
P & C	0.2	2.96	0.08	2.72	-0.02	0.13	---	-3E-3	---	---
Yasada	0.08	2.4	0.1	2.3	---	---	---	---	---	---
S & C	0.15	2.8	0.1	2.5	-0.05	0.25	---	---	---	---

3.4.1   Short Flights

The results of the estimation algorithm for the shorts flights are shown in Table 3-2. Three flights were used together in the estimation algorithm as described in Section 3.3.3. The first six coefficients are in the range of values reported from the wind tunnel studies.

However compared to the Potts and Crowther (2002) data , the differences range from about 40% in the case of C_{Lo} to over 120% for C_{Rr}. Some of this lack of agreement in between estimated coefficients and those determined from wind tunnel tests can be attributed to approximations in the model. For example the Robins-Magnus side force,

neglected here, may cause errors in other coefficients in order to account for motion produced by the neglected force. The variation in the results also can be partially attributed to different Frisbee types, speeds and spin rates tested.
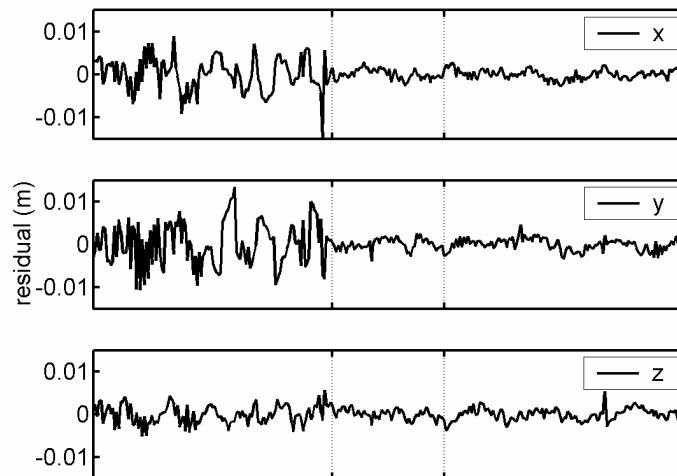

Figure 3-2 Prediction errors in x, y, and z for all three markers for three flights: bsfl5, fffl14, and ffsl5, shown sequentially.

The estimated coefficients do however accurately describe the motion of the atypical flights tested. Residual prediction errors in the x, y, and z components of marker positions are shown for three flights in Fig. 3-2. In the figure, each component of position error for three markers and for three flights is shown on the same axis. The rms position error ranges from about 1 mm to roughly 4 mm. This indicates that the measurement accuracy probably varied between flights. Nevertheless, there is very little correlation observable in the apparently nearly white random noise of the position error traces.

The first six coefficients relate not only to their mean values of lift, drag and pitching moment, but also their sensitivities to angle of attack. In order for their dependence on

angle of attack to be discernible, it is necessary that data be available over a wide range of angles of attack.

Figure 3-3 illustrates the calculated angle of attack time histories for the three flights, shown consecutively. Although the angles of attack of the second flight (fffl14) varied over a very small range (only about 5°), the entire ensemble of three flights experienced angles of attack spanning roughly $0° < \alpha < 30°$, and this provided enough information for a robust determination of the six coefficients associated with angle of attack. This
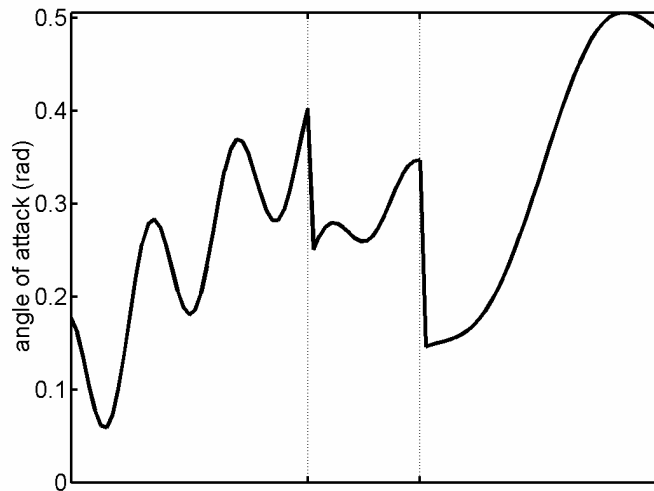

Figure 3-3 Angle of attack versus time for three flights: bsfl5, fffl14, and ffsl5 shown sequentially. Wide range of angle of attack is essential for accurate coefficient estimates.

illustrates an important feature of the estimation algorithm. Although it is difficult in practice to obtain data for a single flight with large variations in angle of attack, this failure can be compensated by data from other flights.

3.4.2 Long Flights

The optimization results for the long flights data are shown in Table 3-2. The three coefficients, C_{Mq}, C_{Rp} and C_{Nr}, found in this experiment vary as much as 80% from the short flights data. It was found that while the coefficients found from the short flight data accurately reflected the short flights, they are not representative of the long flights. This will be discussed further in Section 3.5.

Residual prediction errors in the x, y, and z components of marker positions are shown in Fig. 3-3 for one flight, f2302. The overall rms error of this flight was 1.2 cm.
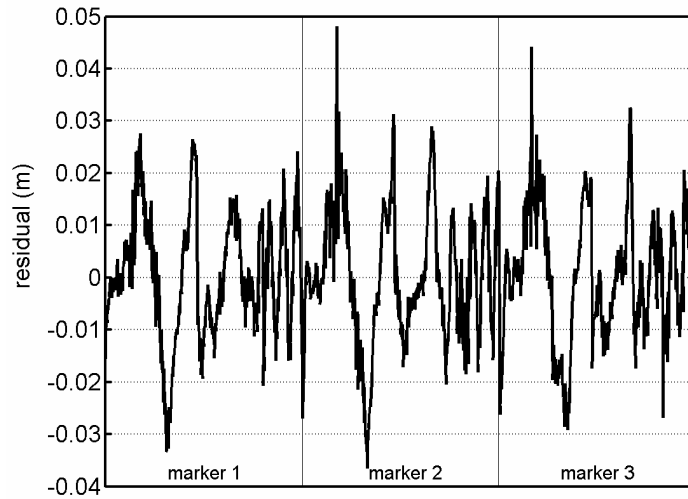

Figure 3-4 Residual error of markers 1, 2 and 3 for long flights throw f2302, indicating the xyz residual of the beginning and end of the flight. The order of the residual is as follows for each marker: beginning x, end x, beginning y, end y, beginning z, and end z.

Flight f2302 was 15 m long, the initial speed and spin was 13.5 m/sec and 54 rad/sec respectively. After the initial wobble damped out, the angle of attack for the flight f2302 (Fig. 3-5) increased from 0.03 to 0.11 rad, equivalent to 1.7° to 6.3° respectively.
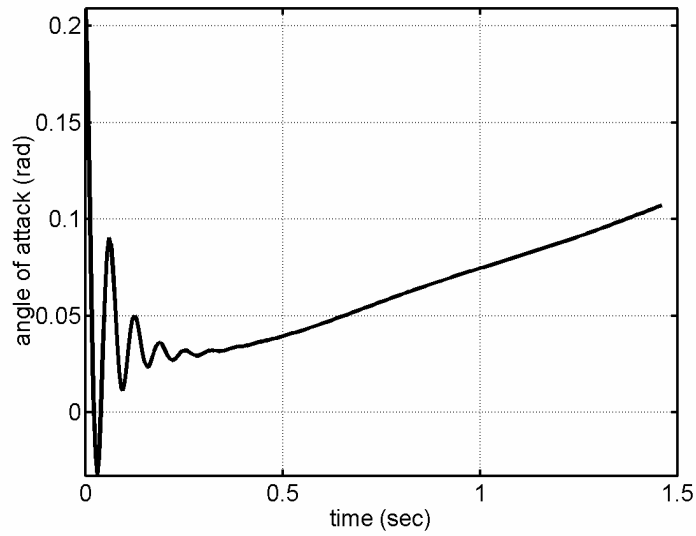
Figure 3-5 Angle of attack vs. time for flight f2302.

3.5 *Discussion*

The validity of the aerodynamic coefficients measured from in-flight data can be shown

with a sequence of flight simulations. Two flights were first simulated using the initial

conditions (Table 3-3) from long flight f2302 (determined from the MATLAB function

fminsearch). The translational state variables of this flight are shown in Fig. 3-6.

Table 3-3 Initial conditions for long flight f2302.

x	y	z	$\dot{x}$	$\dot{y}$	$\dot{z}$	φ	θ	γ	$\dot{\varphi}$	$\dot{\theta}$	$\dot{\gamma}$
m	m	m	m/sec	m/sec	m/sec	rad	rad	rad	rad/sec	rad/sec	rad/sec
-0.90	-0.63	-0.91	13.42	-0.41	0.001	-0.07	0.21	5.03	-14.94	-1.48	54.25

The first simulation (S-1) used the estimated coefficients found from short flights, (Fig.

3-7) while the second simulation (S-2) used the same coefficients, but replaced the three

damping coefficients, C_{Mq}, C_{Rp} and C_{Nr}, with those found using long flights (Fig. 3-8).

Both flights traveled 13.2 m, curved right 1 m and reached a peak height of 1.25 m,

slowing down to 6.5 m/sec at the end of the simulation. The oscillations in φ, θ and their

43
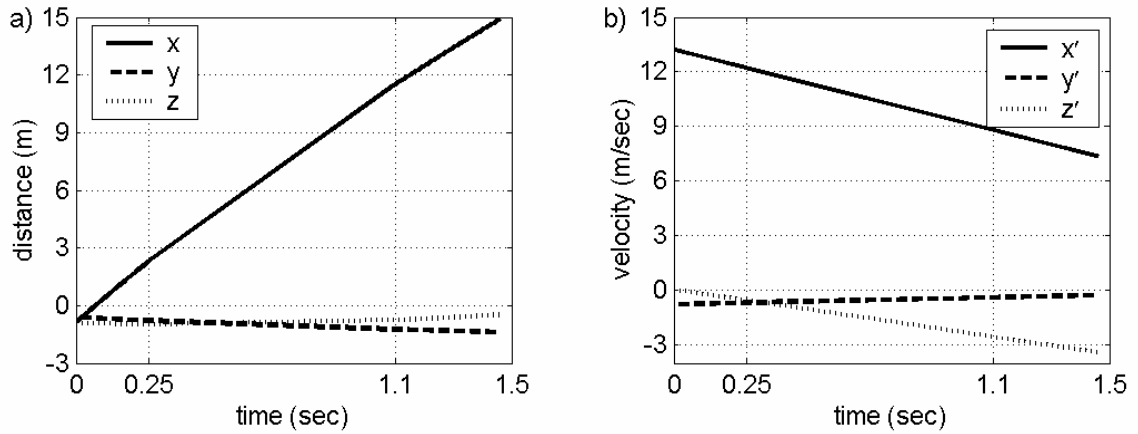
Figure 3-6 Experimental translational states of the flight f2302.

derivatives damped out within 0.25 secs in simulation S-2 while they were still present in

simulation S-1 after 0.5 sec. Thus the results of the two simulations were nearly identical

except for the damping of the φ and θ oscillations.
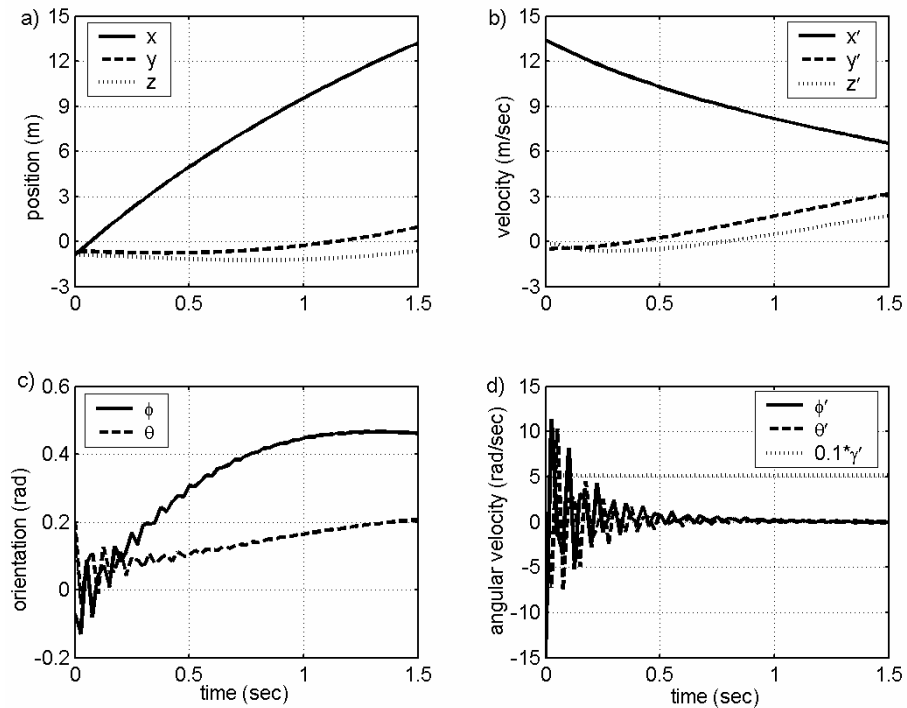
Figure 3-7 State variables of a simulated flight (S-1) using all 10 short flights
aerodynamic coefficients and initial conditions of flight f2302.
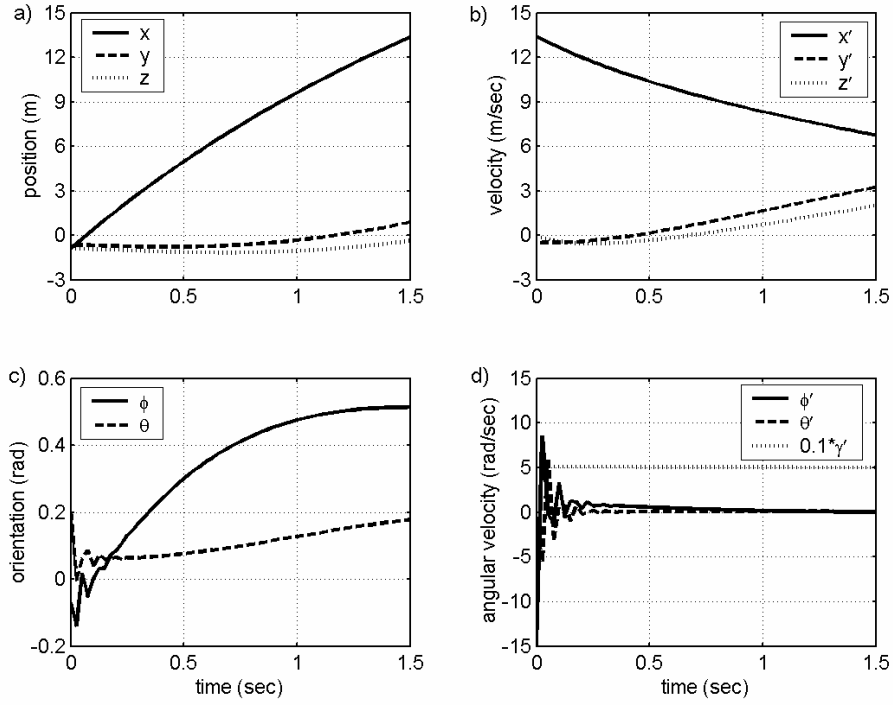
Figure 3-8 State variables of a simulated flight (S-2) similar to simulation (S-1) except using long flights damping coefficients, C_{Mq}, C_{Rp} and C_{Nr}.
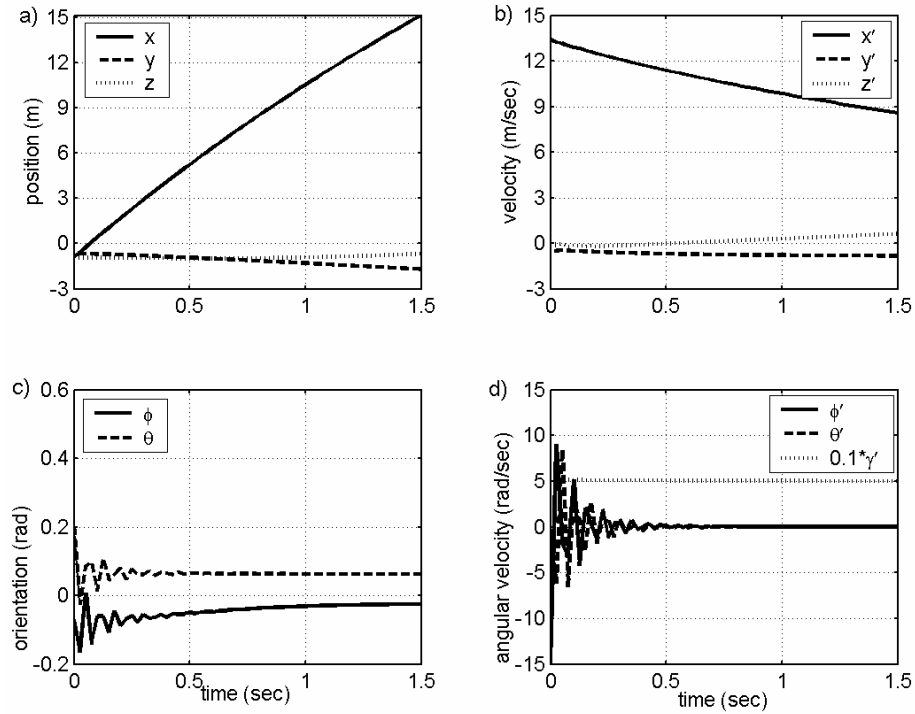

Figure 3-9 State variables of a simulated flight (S-3) using long flights damping coefficients C_{Mq}, C_{Rp} and C_{Nr}, Potts and Crowther values for the other 7, and initial conditions of flight f2302.

A third simulation (S-3) was performed using the values for the lift, drag, and moment coefficients reported by Potts and Crowther (2002) with the values for the damping coefficients found from the long flights optimization (Fig. 3.9). This simulated flight varied considerably from the previous two simulations. Simulation S-3 flied 2 m further, curved 1.7 m to the left rather than to the right, and the velocity in the x direction slowed down to 8.6 m/s, 2.1 m/sec faster than the previous two simulations. The oscillations of φ, θ and their derivatives died out faster than in simulation S-2, but slower than simulation S-1. Also a large change occurred in the φ rotation. After the oscillations damped out, φ maintained a nearly constant 0.06 rad in S-3 but reached a maximum of 0.46 rad in the previous two simulations S-1 and S-2.
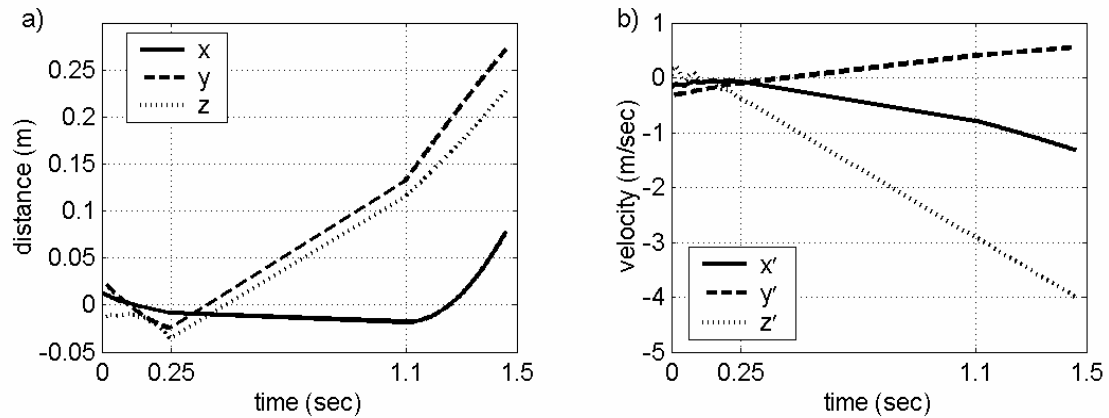

Figure 3-10 Difference in the translational states between the experimental states (Fig. 3-6) and the states simulated using Potts coefficients and the long flights damping coefficients simulation (S-3) (Fig. 3-9).

The translational states of the experimental data for flight f2302 were shown in Fig. 3-6. To compare, the values for the translation states of simulation S-3 and of the flight f2302 were subtracted from each other (Fig. 3-10). The COM position was within 8 cm in the x direction but 27 cm and 23 cm off in the y and z directions respectively. The velocity

error ranges from 0.5 m/sec to -4.0 m/sec. The combination of aerodynamic coefficients reported by Potts and Crowther (2002) together with the long flights damping coefficients provides the most accurate values available for simulating Frisbee flight.

3.6 Conclusions

A method has been presented for the determination of aerodynamics coefficients for the Frisbee that is a practical alternative to time-consuming wind tunnel tests. The method uses an iterative algorithm to find the set of parameters (aerodynamic coefficients and rigid body initial conditions for each flight) that, when used with a numerical simulation model, result in minimum rms position errors between predicted and measured positions for three markers on the Frisbee surface.

Not only does this technique give results comparable to those achieved in the direct measurement of forces and moments, but it is the only practical way of obtaining estimates for certain of the coefficients relating moments about one axis to angular velocities about a second, perpendicular, axis. The accuracy of the estimation algorithm is highly dependent on the accuracy of the measured position data, in the sense that the variances of the coefficient estimates are directly proportional to the mean squared positions measurement noise (Hubbard and Alaways, 1989).

3.7 *Appendix*

In the derivation of the equations of motion, the aerodynamic forces and moments are expressed in reference frame F.

$$\ddot{x} = \frac{\mathbf{F}_{x_F}}{m} \tag{3.9}$$

$$\ddot{y} = \frac{\mathbf{F}_{y_F}}{m} \tag{3.10}$$

$$\ddot{z} = \frac{\mathbf{F}_{z_F}}{m} \tag{3.11}$$

$$\ddot{\varphi} = \frac{\left(\mathbf{M}_{x_F} + I_{xy}\dot{\theta}\dot{\varphi}\sin\theta - I_z\dot{\theta}(\dot{\varphi}\sin\theta + \dot{\gamma}) + I_{xy}\dot{\theta}\dot{\varphi}\sin\theta\right)\cos\theta}{I_{xy}} \tag{3.12}$$

$$\ddot{\theta} = \frac{\left(\mathbf{M}_{y_F} + I_z\dot{\varphi}\cos\theta(\dot{\varphi}\sin\theta + \dot{\gamma}) - I_y\dot{\varphi}\dot{\varphi}\cos\theta\sin\theta\right)}{I_{xy}} \tag{3.13}$$

$$\ddot{\gamma} = \frac{\left(\mathbf{M}_{z_F} - I_z\ddot{\varphi}\sin\theta + \dot{\theta}\dot{\varphi}\cos\theta\right)}{I_z} \tag{3.14}$$

Chapter 4   Torso and Throwing Arm Biomechanical Model for Backhand Frisbee Throw

4.1   Abstract

The flight of the Frisbee is understood but how a person produces the initial conditions remains to be investigated. A seven segment throwing model has been developed to investigate the kinematics and kinetics of backhand Frisbee throws. This model specifies the motion of the torso, allows for the motion of the glenohumeral rhythm and scapular sliding on the thorax, and includes six degrees of freedom: three at the shoulder, and one each at the elbow (ulnahumeral), radioulnar, and wrist (radiocarpal) joints. The equations of motion, developed symbolically using Kane's method, were coded in AUTOLEV. Analysis of 57% maximal effort throws reveals that the largest power contribution results from horizontal adduction of the shoulder providing nearly all the work done to increase translational velocity of the Frisbee. At release the work done by horizontal adduction was 35 J while the total work at all joints was 34 J. The seven segments behaved as a kinetic chain during the throw; however the elbow does not fully extend at any time. It was flexed 57° at release, coming no closer than 27° to full extension during follow through.

4.2 Introduction

More Frisbee's are sold each year than baseballs, basketballs, and footballs combined (Wham-O.com) yet Frisbee related studies remain limited. Technical research on Frisbee dynamics and aerodynamics include wind tunnel studies to measure the aerodynamic lift and drag (Mitchell, 1999; Stilley and Carstens, 1972) and pitching and rolling moments (Potts and Crowther, 2002). Flight simulation and estimation of the aerodynamic force and moment coefficients from in-flight Frisbee data have also been performed (Hubbard and Hummel, 2000; Hummel and Hubbard, 2002). Schuurmans (1990) gave a non-technical description of Frisbee aerodynamics and several books have documented basic throwing techniques (Johnson, 1975; Roddick, 1980). Cotroneo (1980) compared the force contribution of body segments in backhand versus forehand Frisbee throws while inquisitive athletes have qualitatively investigated optimal throwing form, videotaping throwing events to record corresponding Frisbee speed and flight distance (Pozzy, 2002). However, as Frisbee sports have grown and the drive to advance throwing skills has continued, quantitative Frisbee throw biomechanics have been neglected. The flight of the Frisbee is understood but how a person produces the initial conditions remains to be investigated.

The segments of the torso and throwing arm act as a kinetic chain to maximize the speed of the final segment. Kinematic and kinetic studies of arm coordination events (baseball, water polo, and tennis) demonstrate this relationship (Feltner and DaPena, 1989; Feltner and Taylor, 1997; Sprigings et al., 1994). However, many of these studies limit the forearm to a single rigid body rather than two, one for each the radius and the ulna. Also

all exclude motion of the clavicle and scapula shoulder complex relative to the torso. A dynamic model for over-arm throwing including the mechanics of the shoulder has been developed by Cote and Hubbard (2003) but applied only to baseball pitching. No quantitative kinematic or kinetic data was found in the literature for the torso and throwing arm during Frisbee backhand throws.

A seven segment six degrees-of-freedom (DOF) biomechanical model was developed to facilitate kinematic and joint torque analysis of backhand Frisbee throws, including motion of the torso, shoulder, and upper appendage. This work presents a quantitative fundamental understanding of Frisbee throwing biomechanics, focusing on one experienced thrower, rather than studying a larger population. The 3D throwing kinematics were measured and used in an inverse dynamic approach to quantify Frisbee throwing arm kinetics. Because it is possible to achieve this goal with a segmental model and net joint moments, individual muscle force contributions to the joint kinetics were not considered.

4.3   Methods

A previous model of the shoulder (Cote and Hubbard, 2003), composed of the shoulder complex (scapula, clavicle and torso) and the humerus, contained eight DOFs; three rotational DOFs of the shoulder complex, and three rotations and two translations of the humerus. This shoulder model has been incorporated into the Frisbee backhand-throwing model, with several modifications. Humeral head translation within the glenoid fossa is

neglected and the three shoulder complex DOFs are removed as described below. To complete this model the ulna, radius, hand and the three associated DOFs were added.

The Frisbee throwing model thus has six DOFs and seven rigid bodies, the torso, clavicle, scapula, humerus, ulna, radius, and hand/disc. The angles specifying positive rotation are listed in Table 4-1 and are illustrated in Fig. 4-1. Torso motion is specified using measured kinematic data and thus has no dynamic DOFs. Clavicular and scapular motion to position the glenohumeral joint are described by six rotational generalized coordinates and six constraints (three orientation angles of both the clavicle and scapula) which eliminate the dynamic DOFs of these segments. Constraining two points of the scapula to remain in contact with the thorax removes two scapular rotations, θ_4 and θ_6. Longitudinal clavicular rotation, θ_3, is removed by assuming the conoid ligament to be rigid (VanderHelm, 1994). Incorporating three regression equations provides the motion associated with the remaining three DOFs of the shoulder complex. These equations infer clavicle angles θ_1 and θ_2, and the scapular rotation normal to the torso, θ_5, from the humeral angles θ_7 and θ_8 (Cote and Hubbard, 2003), thus providing the shoulder kinematics that cannot be measured using motion analysis.

The 6 dynamic DOFs of the model describe motion associated with the four arm segments about the shoulder, elbow (ulnahumeral), radioulnar and wrist (radiocarpal) joints. The shoulder is modeled as a ball and socket joint with 3 rotational DOFs: θ_7, θ_8, and θ_9. The elbow is represented as a pin joint at the humeral-ulnar articulation to
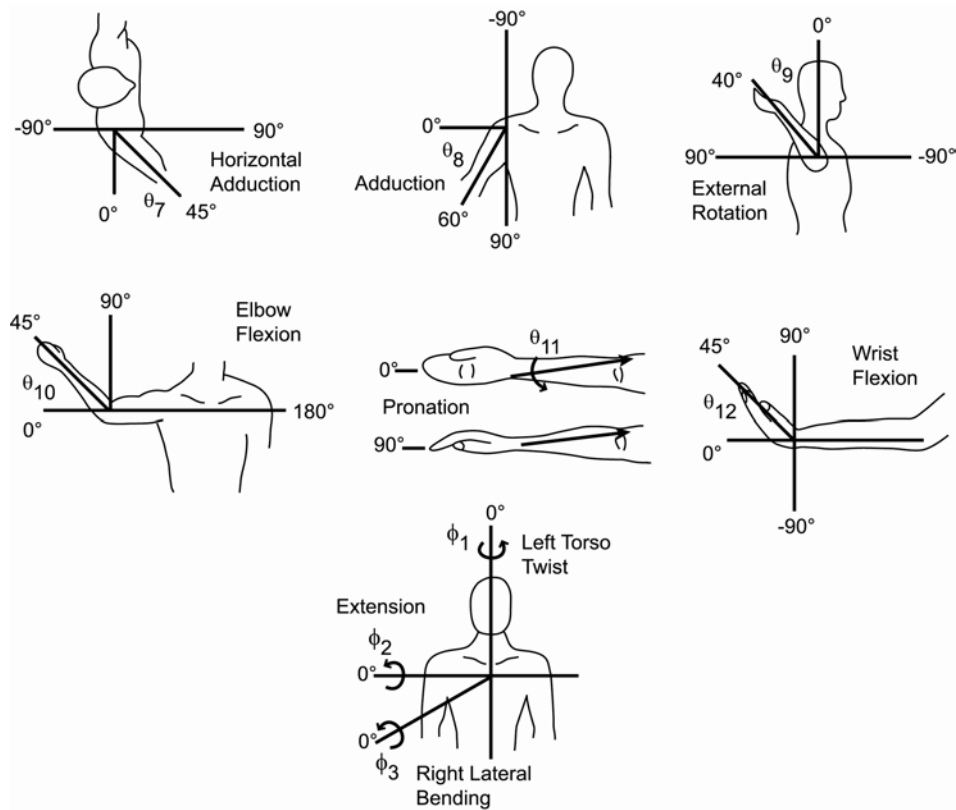
Figure 4-1 Angular rotation sign conventions, labels indicate a positive rotation. Complete naming convention for positive and negative rotations is given in Table 4-1.

Table 4-1 Joint angle sign conventions for positive and negative rotations [A]

Segment	Axis	Angle	Rotation Description		
			Positive angles	*Negative angles*	
torso	z_T	ϕ_1	left torso twist	right torso twist	
	y_T	ϕ_2	right lateral bending	left lateral bending	
	x_T	ϕ_3	extension	flexion	
clavicle		θ_1	protraction	retraction	
		θ_2	depression	elevation	
		θ_3	external rotation	internal rotation	
scapula		θ_4	protraction	retraction	
		θ_5	medial rotation	lateral rotation	
		θ_6	backward tilt	forward tilt	
humerus	z_H	θ_7	horizontal adduction	horizontal abduction	DOF
	y_H	θ_8	adduction	abduction	DOF
	x_H	θ_9	external rotation	internal rotation	DOF
ulna	z_U	θ_{10}	elbow flexion	elbow extension	DOF
radius	$- x_R$	θ_{11}	pronation	supination	DOF
hand/disc	z_D	θ_{12}	wrist flexion	wrist extension	DOF

[A] *Counterclockwise/clockwise references in text refer to view from above*

53

produce elbow flexion, θ_{10}. This axis of rotation is assumed perpendicular to the long axis of the humerus and ulna, neglecting any varus-valgus angle (LeMay and Crago, 1996). Pronation, θ_{11}, of the radius/ulna pair occurs along an axis through the distal and proximal radioulnar joints. This longitudinal axis extends from the center of the distal ulna through the proximal radial head (Gonzalez et al., 1996). The wrist is modeled as a pin joint between the radius and the carpal bones of the wrist (LeMay and Crago, 1996) to produce flexion at the wrist, θ_{12}, about an axis perpendicular to the axis of pronation. Wrist abduction/adduction is neglected.

Four 180 Hz motion capture cameras (Motion Analysis Inc., Santa Rosa, CA) recorded motion of reflective markers positioned on the subject and Frisbee. xyz coordinates were calculated using direct linear transformation methods (DLT) (Shapiro, 1978). Exact resolution of the system is not known, but the iterative estimation algorithm described below had an rms error of 9 mm. The test procedure included unlimited time for warm-up, a static measurement, and backhand throws of an experienced right-handed male subject (from whom informed consent was provided). The subject was encouraged to throw with maximum effort using an Ultimate Frisbee regulation disc (DisCraft UltraStar mass: 175g, diameter: 27 cm). Initially the thrower stood with hands by his side and his torso x-axis not parallel to the throwing direction x_N, but rotated 20° to the right. The subject then performed the throw and brought his hand back to the original position. Approximate positions of the body segments at release are shown in Fig. 4-2. Three or more non-collinear markers were arranged on each body segment, 14 markers total. Five additional markers were used during the static test to allow tracking of four virtual joint

54

center markers throughout the throwing trials. The virtual joint centers served as the origin for the body fixed coordinate systems. The static test also enabled determination of all intramarker distances.

Analysis of each trial included 1.25 seconds before till 1 second after release; release occurred at time t = 0. Three markers were attached to the top plane of the Frisbee. The release frame was estimated visually from analysis of the video data. After tracking, the xyz coordinate marker data were smoothed with a 10 Hz butterworth filter. Seven throws performed during the testing procedure where chosen for analysis. Additional trials were not acceptable due to excessive missing marker data during the motion capture.

Several approaches exist for improving the accuracy of inverse dynamic computations (Kuo, 1998). A technique similar to that described by Miller et al. (1980) was used to obtain segmental kinematic rotations (θ_7 - θ_{12}) from the motion analysis data. Noise from the system and marker movement on the skin during the throw was removed from the measured xyz coordinate data through an iterative estimation algorithm. This algorithm estimated nine parameters: the xyz coordinates of the shoulder joint center and the six angular DOFs. It calculated the predicted xyz marker positions that best matched the experimental marker data, while satisfying the throw model configuration assumptions including constant segment lengths. The algorithm's general method included:

1. Using current value of the nine parameters, predict the xyz coordinates of all markers based on the segment model, (for the first time frame the measured xyz coordinates were used as an initial guess).

2. Calculate the residual r between the predicted and measured xyz marker coordinates for a single frame.

$$r = \sum_{i=1}^{3} \sqrt{(x_p - x_m)_i^2 + (y_p - y_m)_i^2 + (z_p - z_m)_i^2} \qquad (4.1)$$

3. Calculate both the gradient and Hessian of the residual with respect to the vector of parameters.

4. Determine a correction/adjustment to each of the nine parameters that reduces the residual using the method of Hubbard and Alaways (1989).

5. Return to step 2 until the residual reaches a minimum.

6. Repeat steps 1-5 for each time frame.

The estimated marker positions were used to establish and track right handed orthogonal coordinate systems aligned along the segment principal axes. The location of the shoulder, elbow, and wrist joint centers were calculated as a point halfway between two markers placed along the rotational axis, y_H, z_U and z_D respectively. The proximal ulna, and proximal and distal radial joint center locations were translated from the surface markers along the respective axes. Each joint center location was then calculated and tracked with respect to three other segment fixed markers for each frame.

The inertial reference frame, N, has z_N vertical, x_N horizontal in the throw direction, and $y_N = z_N \times x_N$ (Fig. 4-2). The torso reference frame T is aligned with the inertial frame for zero torso rotations. The x_T, y_T and z_T directions were associated with the
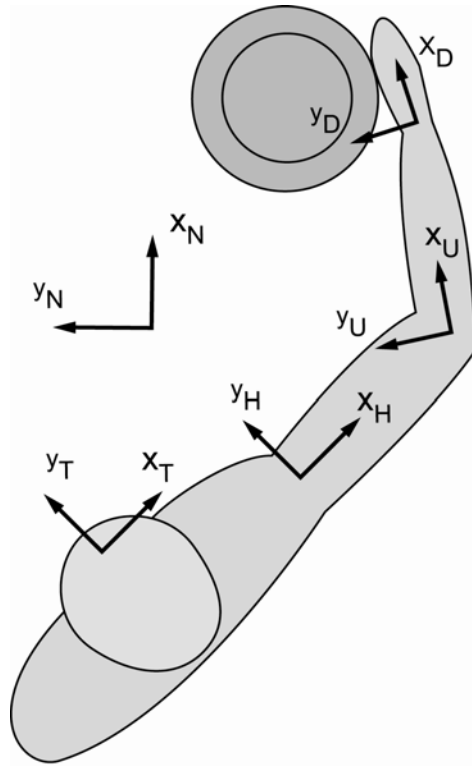
Figure 4-2 Top view of inertial and segment reference frames of throwing arm, x_N is the direction of throw, relative positions shown at release.

extension/flexion, right/left lateral bending, and left/right twist of the torso, respectively.

By definition, for zero twist the thrower will be facing perpendicular to the throwing

direction.

The body fixed reference frames of the humerus, ulna, radius and disc/hand (H, U, R, and

D respectively) were constructed similarly, x along the longitudinal axis, y in the

transverse plane pointed medially and $z = x \times y$. The x_H, y_H and z_H directions were

associated with the external/internal rotation, adduction/abduction, and horizontal

adduction/adduction at the shoulder, respectively. Alignment of the torso and humeral

coordinate systems coincides with 0° adduction when the arm is perpendicular to the

57

torso and 90° when at the side. The y_U and z_U directions were associated with valgus/varus rotation and flexion/extension at the elbow, respectively. The $-x_R$ direction corresponds to pronation/supination and z_D is associated with wrist flexion/extension. Details for defining the axes of segment reference frames are included in the appendix.

Joint angles were calculated from components of the transformation matrices between adjacent segment reference frames. Joint angle definitions for positive measurement are shown in Table 4-1. $^{T}T^{N}(t)$ is the transformation matrix between the inertial reference frame and the torso fixed frame at each time frame, and $^{H}T^{T}(t)$ is the similar transformation between the humerus and torso frames. Both transformations correspond to a Euler body 3-2-1 rotation sequence (Kane and Levinson, 1996) of ϕ_1, ϕ_2, ϕ_3, and $\theta_7, \theta_8, \theta_9$, respectively.

$$\text{For } [\mathbf{T}] = \begin{bmatrix} T_{11} & T_{12} & T_{13} \\ T_{21} & T_{22} & T_{23} \\ T_{31} & T_{32} & T_{33} \end{bmatrix} \tag{4.2}$$

$$\phi_1 = \frac{\sin^{-1} {}^{T}T^{N}_{12}}{\cos\phi_2} \tag{4.3a}$$

$$\theta_7 = \frac{\cos^{-1} {}^{H}T^{T}_{11}}{\cos\theta_8} \tag{4.3d}$$

$$\phi_2 = -\sin^{-1} {}^{T}T^{N}_{13} \tag{4.3b}$$

$$\theta_8 = -\sin^{-1} {}^{H}T^{T}_{13} \tag{4.3e}$$

$$\phi_3 = \frac{\sin^{-1} {}^{T}T^{N}_{23}}{\cos\phi_2} \tag{4.3c}$$

$$\theta_9 = \frac{\cos^{-1} {}^{H}T^{T}_{33}}{\cos\theta_8} \tag{4.3f}$$

$^{U}T^{H}(t), {}^{R}T^{U}(t),$ and $^{D}T^{R}(t)$ are the transformations for simple rotations of the ulna in H about z_H, the radius in U about $-x_R$, and the wrist in R about z_R, respectively. Thus the remaining DOFs of the model were calculated from:

$$\theta_{10} = \cos^{-1} {}^{U}T_{11}^{H} \tag{4.4a}$$

$$\theta_{11} = \cos^{-1} z_H \bullet z_R \tag{4.4b}$$

$$\theta_{12} = \cos^{-1} {}^{D}T_{11}^{R} \tag{4.4c}$$

All angle data were smoothed using a MATLAB cubic spline smoothing function
(SPAPS) with a tolerance of 0.004. Angular velocities and accelerations were calculated
as first and second derivatives respectively of the angular displacements.

The model was implemented in AUTOLEV, a symbol manipulation program (Kane and
Levinson, 1996), to derive the equations of motion (EOM) expressing acceleration in
terms of the joint torques and specified torso motion (computer code included in the
thesis appendix). Using inverse dynamics, the EOMs were solved for the torques, with
body segment parameters and segment kinematics as inputs. Segment mass, inertia and
center of mass locations (Table 4-2) were taken from Veeger et al. (1991). Power
associated with each DOF was calculated as the product of torque and the corresponding
relative angular velocity of the joint. Work done by each DOF was calculated as the

Table 4-2 Segment Properties (Veeger et al., 1991)

Segment	Mass (kg)	Inertia (I_x) (kg m^2)	Inertia (I_y, I_z) (kg m^2)	% cm position[A]	Length (m)
torso	-	-	-	-	-
clavicle[C]	0.31	-	-	0.50	0.15
scapula[C]	0.69	-	-	-	0.15
humerus	1.72	0.0013	0.0143	0.53	0.35
ulna[D]	0.52	0.0001	0.0041	0.39	0.27
radius[D]	0.52	0.0001	0.0041	0.39	0.27
hand[B]	0.46	0.0002	0.0006	0.40	0.11
disc	0.175	0.00122	0.00122, 0.00235	0.50	0.27

[A] Ratio of segment length measured from proximal end. [B] Hand and disc were treated as
one segment until release. [C] Approximation of Veeger torso data (Cote and Hubbard,
2003). [D] Approximation of Veeger forearm data (Lemay and Crago, 1996).

integral of the total power. This calculation included work done at the upper extremity joints only, therefore not including work done by the torso and legs.

4.4 Results

The release conditions of the seven analyzed trials had an average initial speed of 12.7 m/sec with a 0.92 standard deviation and an initial spin rate of 46.5 rad/sec, standard deviation of 3.7. Radar gun measurements of the subject's throwing speed outside of the testing environment revealed maximum effort to be 22.4 m/sec. Thus the 7 throws can be categorized as 57% of maximum effort.

4.4.1 Qualitative Kinematics

The Frisbee throwing motion can be divided into three phases, based on the maximum and minimum range of the torso twist angle (Fig. 4-3A): 1) wind-up 2) acceleration and 3) follow through. Wind-up begins when the torso starts to twist left (counterclockwise viewed from above) away from the target. The weight of the thrower shifts to the left foot and the arm horizontally adducts, drawn towards the torso, while the forearm flexes and the wrist curls around the disc.

The acceleration phase, characterized by sequential uncoiling of the torso and arm segments, begins when the torso has reached its maximum rotation to the left. As the torso twists right, the torso bends forward and right laterally as the weight shifts from

the left to right foot. During this phase maximum ranges of torso left rotation, shoulder adduction, elbow flexion and wrist flexion occur.

When the Frisbee is released, the torso is tilted forward, the humerus and torso x axes are nearly aligned, and the arm is externally rotating at the shoulder. The forearm is pronating and the elbow is not fully extended. However, the wrist is fully extended. After release, the arm continues to extend at the shoulder, elbow and wrist. Follow through is completed when the torso reaches maximum right twist.

4.4.2 Quantitative Kinematics

Average angular displacement data of the torso, humerus, ulna, radius, and hand for seven throws are shown in Fig. 4-3. Segmental angular displacement and angular velocities at maxima/minima and time of release are presented in Table 4-3.

The torso x_T axis is originally offset from the throwing direction by -20°. During wind-up the torso twists left 14° (clockwise viewed from above) reaching a maximum left twist of -6°. The torso then switches direction, signifying the onset of the acceleration phase, by twisting right, continuing through release at -42° to –69°, a total range of motion of 63° by the end of follow through. Meanwhile the torso flexes 27° steadily forward and bends 7° laterally right throughout the wind-up, acceleration and follow through phases.
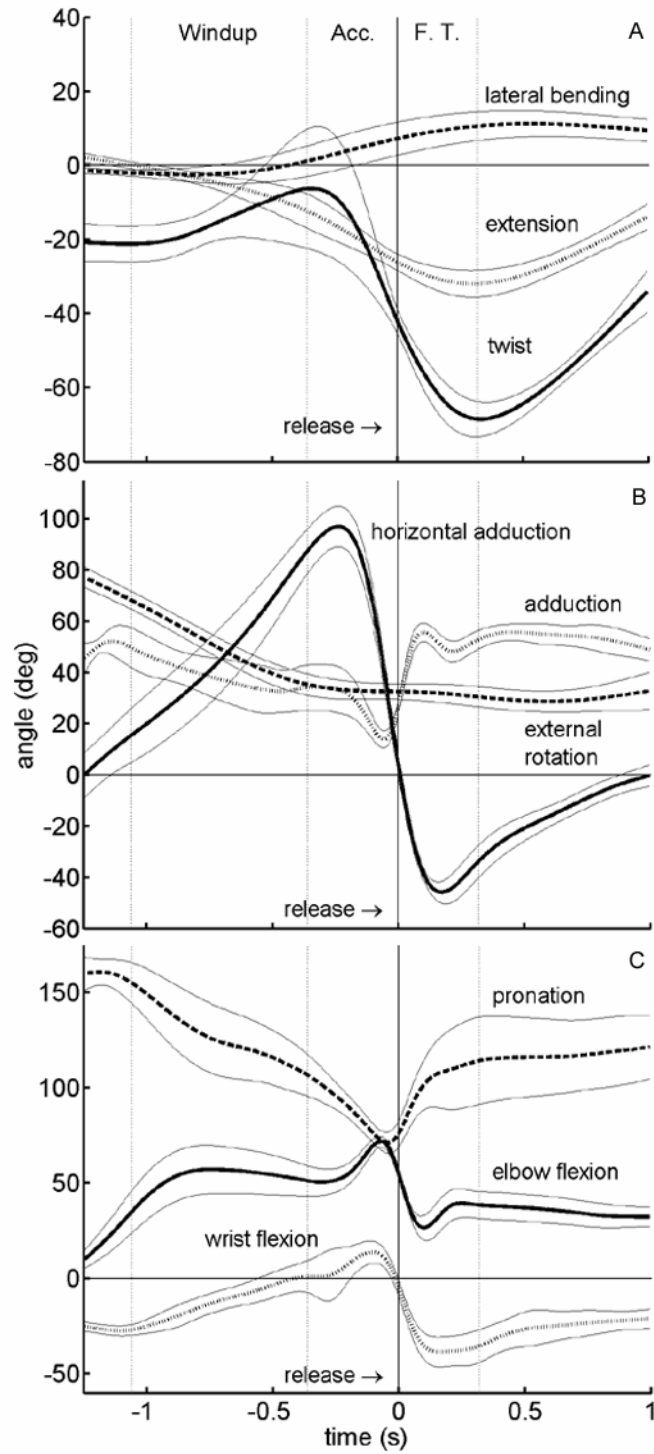
Figure 4-3 A) Torso rotations, where positive extension corresponds to the torso bending backwards B) Humerus rotations and C) Ulna, radius and hand rotations during the three phases of Frisbee throwing: Wind-up, Acceleration (Acc.) and Follow Through (F.T.). Shown with ±1 standard deviation (n=7) indicated.

Table 4-3 Angular displacement and angular velocity at peak and release values during acceleration and follow through phases.

axis			Angular Displacement				Angular Velocity		
			deg				*deg/sec*		*sec*
axis			*max*	*min*	*diff*	*at release*	*at release*	*peak*	*time*
Torso									
z_T	ϕ_1	left twist	-6	-69	63	-42	-155	-168	-0.06
y_T	ϕ_2	right lateral bending	11	1	10	7	15	18	-0.22
x_T	ϕ_3	torso extension	-12	-33	21	-27	-36	-42	-0.13
Humerus									
z_H	θ_7	horizontal adduction	97	-46	143	3	-599	-653	-0.04
y_H	θ_8	adduction	55	14	41	27	434	477	-0.03
x_H	θ_9	external rotation	35	31	4	33	-2	-1	0.02
Ulna									
z_U	θ_{10}	elbow flexion	72	27	45	57	-431	-447	0.03
Radius									
- x_R	θ_{11}	pronation	114	71	43	76	224	308	0.06
Hand/disc									
z_D	θ_{12}	wrist flexion	14	-38	52	-5	-379	-397	0.04

The greatest range of motion, 143° total (Fig. 4-3B), and highest peak angular velocity occurs at the shoulder joint due to horizontal adduction/abduction. Nearly 100° range of motion occurs in horizontal adduction during windup and acceleration. At release horizontal adduction is near zero indicating the x_H and x_T axes are nearly parallel. Then approximately 50° range of motion occurs in horizontal abduction during follow through. During acceleration, horizontal abduction achieves a maximum rate of 653°/sec. The range of motion of external rotation is small (14° to 56°) but the rate is 434°/sec at release. Adduction decreases to 35° during wind-up and deviates less than 5° throughout acceleration and follow through.

Elbow flexion remains relatively constant near 50° during wind-up. Midway through acceleration but after peak horizontal adduction, elbow flexion peaks at 72° before decreasing to 27° after release. At release, the elbow is flexed 57° and has an angular velocity of 431°/sec. in extension. The forearm position starts near 150° pronation, rotating in supination throughout wind-up and during most of acceleration, then begins pronating 0.05 sec before release from 71° to 114° during follow through. Wrist flexion gradually increases during wind-up until midway through the acceleration phase. Wrist range of motion is 52° total from 14° to –38°. At release the wrist is 5° past full extension, extending at 379°/sec.

4.4.3 Kinetics

The peak torques and power, and the torque, power and work done at release for each rotation are shown in Table 4-4. Peak torques (Fig. 4-4) range from 36 and 34 Nm for adduction and horizontal adduction, respectively, to 1 and –12 Nm for wrist flexion/extension and external/internal rotation respectively. At release, power stems predominately from the horizontal abduction, 115 W (Fig. 4-5) which, 0.04 seconds prior reached a peak of nearly twice that, 312 W. This provides for the total kinetic energy to reach a maximum at release. The positive power generated by horizontal abduction is accelerating the upper appendage up through release then decelerating the upper appendage after release through negative power. Wrist flexion contributes a small amount of power 8 W at release, while all the other torques constrain the acceleration of the arm.

For example the elbow flexion torque is positive 12 N m at release, decelerating the

forearm and resulting in negative power contribution.

Table 4-4 Peak joint torques, Peak Power, and their respective times; torque, power and
work at release.

			Peak Torque and time		Peak Power and time		*at release*		
							Torque	Power	Work
			N m	*sec*	*W*	*sec*	*N m*	*W*	*J*
Humerus									
z_H	θ_7	horizontal adduction	34	0.08	312	-0.04	-25	115	35
y_H	θ_8	adduction	36	0.05	6.1	-0.74	13	-0.8	4.2
x_H	θ_9	external rotation	-12	0.04	-90	0.03	-4.7	-35	-1.2
Ulna									
z_U	θ_{10}	elbow flexion	17	0.06	-137	0.03	12	-125	-4.0
Radius									
- x_R	θ_{11}	pronation	7.7	0.04	-0.5	0.07	4.9	-0.2	-0.2
Hand/disc									
z_D	θ_{12}	wrist flexion	1.4	0.03	11	0.02	1.1	8.0	0.2
								Total	34

The total work done by the arm joints at release is 35 J, more than twice the Frisbee's

kinetic energy at release (Fig. 4-6). Average Frisbee speed and spin at release are 12.7

m/sec and 46.5 rad/sec, respectively. Frisbee total kinetic energy is 16.8 J at release, of

which 14.3 J is translational and 2.5 J is rotational kinetic energy. The relatively small

ratio of rotational to translational kinetic energy is due to the fact that the spin parameter,

$S = r\omega / v$ is only 0.49. The coordinated joint torques produce an angular velocity of the

Frisbee nearly in line with its spin axis, and a velocity vector near the plane of the

Frisbee, thus the angle between the velocity vector and the Frisbee plane is small, 0° to

15°.
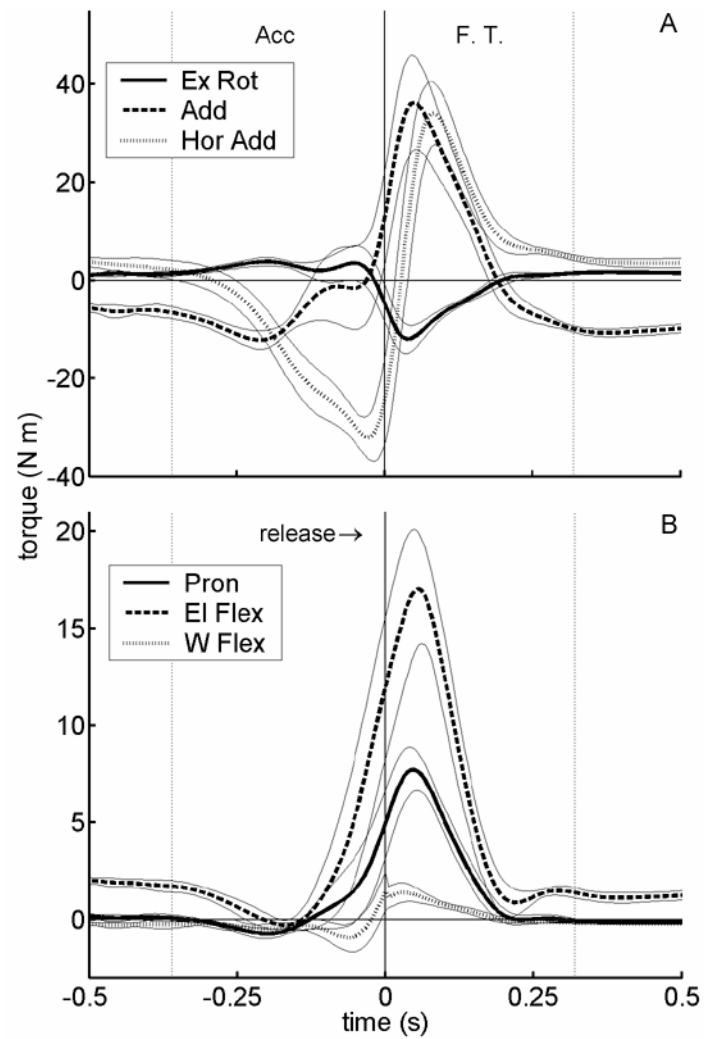
Figure 4-4 A) Shoulder and B) Elbow and Wrist Joint Torques during the last two phases of Frisbee throwing: Acceleration (Acc) and Follow Through (F.T.).
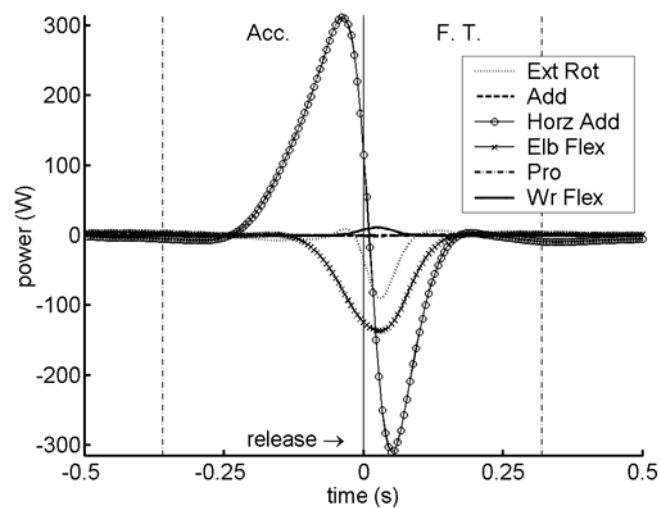
Figure 4-5 Power of each DOF during the last two phases of Frisbee throwing: Acceleration (Acc) and Follow Through (F.T.).
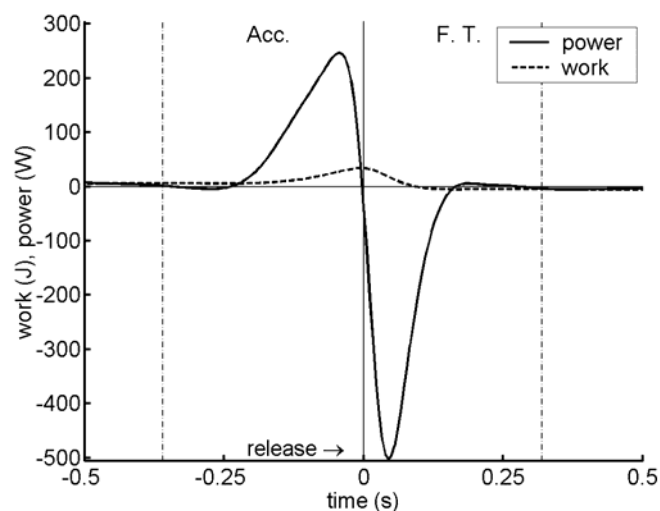
Figure 4-6 Total Power and Work during the last two phases of Frisbee throwing: Acceleration (Acc) and Follow Through (F.T.).

4.5   Discussion

The data presented were based on the analysis of one thrower. It is unknown whether the

results are representative of a larger group of Frisbee throwers.

67

Frisbee throws partially demonstrate the kinetic chain principle which states that peak angular velocities occur in a sequence from proximal to distal segments to generate maximum velocity at the end point (Krieghbaum and Barthels, 1996; Putnam, 1993). Peak torso twist rate occurs at –0.06 seconds followed by peak horizontal abduction, elbow and wrist extension rates at –0.04, 0.03 and 0.04 seconds respectively. In a kinetic chain, during acceleration of the proximal segment the adjacent distal segment lags behind. This is observed with the upper arm and forearm (Fig. 4-3). When the humerus begins horizontal abduction, elbow flexion begins to increase. However, in a kinetic chain all segments are contributing positive power, this is not the case with the Frisbee throw. Positive power is generated mainly by horizontal abduction and slightly by wrist flexion. However the power contribution from elbow flexion is negative throughout the throw, reaching a peak of -137 W after release. The negative power acts to decelerate the forearm, preventing a whip-like effect that may be observed in a kinetic chain.

Beginning throwers are often instructed to focus on increasing their wrist snap, but analysis of the Frisbee throw suggests otherwise. At release the power and work done at the wrist are only 8 W and 0.2 J respectively while the main components of power and work occur at the shoulder from horizontal abduction. The work done at release by horizontal abduction is 35 J while the total work of the joints is 34 J. This implies that novice throwers might experience larger improvements by instead concentrating on increasing the power at the shoulder by increasing the horizontal abduction rate. This increase in torque and angular velocity may translate, through the kinetic chain, to the wrist. While wrist snap, may be important for imparting maximum angular velocity to the

68

Frisbee, it is possibly of secondary importance to Frisbee translational velocity for the beginning thrower.

The configuration of the thrower at release may be dependent on subconscious factors. At release the torso x axis, x_T, is rotated 42° clockwise past the direction of the throw. The x_T and x_H axes are offset by only 3°, the elbow is flexed 57° and the wrist is 5° past full extension (Fig. 4-2). During the follow through, elbow extension reaches a maximum but still comes no closer than 27° to full extension. Non-full extension of the elbow during the throw suggests a subconscious reflex may be present. The configuration at release allows the thrower to somewhat face the throw direction, but does not allow maximum range of motion of horizontal abduction and elbow extension. Releasing the Frisbee when the elbow is closer to full extension might be more conducive to generating higher Frisbee velocity, however this configuration also would increase the risk of hyperextension and injury to the elbow. Subconscious protection mechanisms seem to inhibit full extension. This has been observed in other throwing events including baseball. Feltner and DePena (1986) found that at maximum extension the elbow is still 20° from full extension.

While the standard deviations are consistently narrow at release for all angles (Fig. 4-3), they vary widely throughout the throw. For example, torso twist standard deviation is as large as 25° 0.25 seconds before release but decreases to only 7° by release. This suggests that for 57% maximal effort throws, the torso twist range of motion may not heavily influence conditions at release. The small standard deviation at release for all

69

DOFs, however, implies there may be a preferred configuration by the thrower, even at submaximal effort.

The kinematics and kinetics of the segments of the upper appendage have been presented. Frisbee throws result in nearly 140° horizontal abduction, 100° of which occurs before release. The elbow does not fully extend at any time during the throw. The negative power generated serves to decelerate the forearm and hand due to a possible subconscious reflex to prevent hyperextension. The positive power for the throw is primarily generated by horizontal abduction. Positive power can be maximized by facing perpendicular to the throw direction to allow for maximum range and angular velocity of horizontal abduction prior to release.

4.6 Appendix

4.6.1 Marker Sets

The marker sets used during the Frisbee throwing data collection procedures are listed in

Table 4-5. 17 markers were used during the throwing trials. Prior to testing a static test

was performed which included the markers of the trial data collection plus an addition 5

markers. After data collection, the positions of 4 virtual markers were calculated. The

markers did not really exist but their positions relative to other markers on the segment

could be calculated for the entire time interval of the trial.

Table 4-5 Marker set for Frisbee throwing data collection.

Trial Markers	Additional Static Test Markers	Virtual Markers
left top shoulder	lateral elbow	shoulder joint center (JC)
right top shoulder	medial elbow	elbow joint center (JC)
top sternum	front shoulder	wrist joint center (JC)
middle sternum	back shoulder	center of mass of Frisbee
left rib	radioulna	
right rib		
deltoid		
bicep*		
arm		
forearm		
right wrist*		
left wrist*		
distal radius		
knuckle		
Frisbee1		
Frisbee2		
Frisbee3		

These markers were attached to 2-3 cm long rods and strapped to the subject.

4.6.2　Definitions of segment coordinate systems

Inertial Reference Frame N

Up:　　　z_N　= Vertical

Forward:　x_N　= Horizontal in the direction of throw

Right:　　y_N　= $z_N \times x_N$

Intermediate Torso Reference Frame T'

The rotation of the torso was calculated by defining two coordinate systems fixed in the

torso, designated T' and T. The intermediate coordinate system T' is fixed with respect to

the markers on the torso and thus has an arbitrary alignment in the torso. This coordinate

system can be calculated with respect to N at all times intervals from the torso marker

positions.

Origin: Halfway between the left and right rib markers

$\quad\quad x_{T'}$　= Vector from torso origin to the right rib marker

$\quad\quad y_{T'}$　= Vector from torso origin to top sternum $\times$ $x_{T'}$

$\quad\quad z_{T'}$　= $x_{T'} \times y_{T'}$

Torso Reference Frame T

Defines a coordinate system T fixed along the long and short axes of the torso. Calculated

from the markers at the first time frame when subject is standing straight up. Subsequent

position of the reference frame T is calculated relative to the intermediate torso frame T'

describe above.

Origin: Halfway between the two rib markers

Lateral: x_T = Vector from torso origin to left rib marker – z_N component

Anterior: y_T = x_T ✕ vector from right rib to left rib

Superior: z_T = x_T ✕ y_T

Humerus Reference Frame H

Distal: x_H =Vector from shoulder JC to elbow JC

z_H = x_H ✕ x_U

Medial: y_H = z_H ✕ x_H

Ulna Reference Frame U

Distal: x_U =Vector from ulna JC to wrist JC

Medial: z_U = x_H ✕ x_U

Radius Reference Frame R

Distal: x_R =Vector from proximal radius JC to distal ulna JC

z_R =Vector from wrist JC to distal radius, but perpendicular to x_R

Medial: y_R =-x_R ✕ z_R

<u>Hand Reference Frame</u>

Distal: x_D =Vector from wrist JC to knuckle, but perpendicular to z_R

The axis of rotation ($-x_R$) for pronation is approximately 14° off of the long axis of the

ulna, x_U. This vector ($-x_R$) extends from distal ulna joint center to the proximal radius

joint center

4.6.3   Calculation of joint centers and virtual markers

The joint centers of the shoulder, elbow, and wrist were found as the halfway point on an

axis between two markers whose positions were visually estimated,

  JC shoulder   = ½ (front shoulder+ back shoulder)

  JC elbow   = ½ (lateral elbow + medial elbow)

  JC wrist   = ½ (distal radius + radioulna)

Virtual markers locations where calculated relative to the location of three other markers

on the same segment during a static reference measurement. The three markers are used

to calculate a virtual coordinate frame and the location of the virtual marker in this frame.

Thus the virtual markers were not viewed/on during the actual Frisbee throw, but the

reference markers remained in place during the trials, the virtual markers positions could

also be calculated during the trials. The shoulder JC, elbow JC, lateral elbow, and medial

elbow virtual markers were calculated using the following reference markers

Origin: deltoid

Y axis: arm

XY plane: bicep

The wrist JC, radioulna and distal radius virtual markers were found using the following
reference markers:

Origin: forearm

Y axis: left wrist

XY plane: right wrist

References

Anderson, J.D., 2001. Fundamentals of aerodynamics (3rd ed.). McGraw-Hill, Dubuque, Iowa.

Bloomfield, L.A. (1999, April). The flight of the Frisbee. *Scientific American,* 132.

Cote, D.D., Hubbard, M., 2003. An 8 DOF lumped-parameter model of shoulder motion including glenohumeral translation and scapular motion. J. Biomechanics, submitted.

Cotroneo, P.W. (1980) Biomechanical and aerodynamical aspects of the backhand and sidearm Frisbee-disc throws for distance. MS thesis, California State University, Hayward.

Etkin, B., Reid, L.D., 1996. Dynamics of Flight: Stability and Control. John Wiley and Sons, New York.

Feltner, M., DaPena, J., 1986. Dynamics of the shoulder and elbow joints of the throwing arm during a baseball pitch. Int. J. Sports Biomechanics 2, 235-259.

Feltner, M., DaPena, J., 1989. Three dimensional interactions in a two-segment kinetic chain. Part1: General model. Int. J. Sports Biomechanics 5, 403-419.

Feltner, M.E., Taylor, G., 1997. Three-dimensional kinetics of the shoulder, elbow and wrist during a penalty throw in water polo. J. Applied Biomechanics 13, 347-372.

Frolich, C., 1981. Aerodynamic effects on discus flight. American Journal of Physics 49, 1125-1132.

Ganslen, R.V., 1964. Aerodynamic and mechanical forces in discus flight. Athletic Journal 44(50).

Gonzalez, R.V., Hutchins, E.L., Barr, R.E., Abraham, L.D., 1996. Development and

    evaluation of a musculoskeletal model of the elbow joint complex. J.

    Biomechanical Engineering 118, 32-40.

Hubbard, M., Alaways, L.W., 1989. Rapid and accurate estimation of release conditions

    in the javelin throw. J. Biomechanics 22(6/7), 583-595.

Hubbard, M., Hummel, S.A. 2000. Simulation of Frisbee flight. In Proceedings of the 5th

    Conference on Mathematics and Computers in Sports, University of Technology,

    Sydney, Australia.

Hummel, S.A., Hubbard, M. 2002. Identification of Frisbee aerodynamic coefficients. In

    Proceedings of the 4th International Association Conference on Engineering in

    Sports, Kyoto, Japan.

Johnson, S.E.D., 1975. Frisbee: A practitioners manual and definitive treatise. Workman

    Publishing Company, New York.

Kane, T.R., Levinson, D.A., 1996. Dynamics Online: Theory and Implementation with

    AUTOLEV. Online Dynamics, Inc.

Krieghbaum, E., Barthels, K.M., 1996. Biomechanics: a qualitative approach for studying

    human movement (4th ed.). Allyn and Bacon, Needham Heights.

Kuo, A.D., 1998. A least-squares estimation approach to improving the precision of

    inverse dynamics computations. Journal of Biomechanical Engineering 120, 148-

    159.

LeMay, M.A., Crago, P.E., 1996. Dynamic model for simulating movements of the

    elbow, forearm and wrist. J. Biomechanics 29, 1319-1330.

Lissaman, P. (1993). Stability and dynamics of a spinning oblate spheroid. Unpublished
  Manuscript.

McCormick, B.W., 1995. Aerodynamics Aeronautics and Flight Mechanics (2nd ed.).
  John Wiley and Sons, New York.

Meriam, J.L., Kraige, L.G., 1992. Engineering Mechanics - Dynamics (3rd ed.) (Vol. 2).
  John Wiley and Sons, New York.

Miller, N.R., Shapiro, R., McLaughlin, T.M., 1980. A technique for obtaining spatial
  kinematic parameters of segments of biomechanical systems from
  cinematographic data. J. Biomechanics 13, 535-547.

Mitchell, T.L. (1999) The aerodynamic response of airborne discs. MS thesis, University
  of Nevada, Las Vegas.

Panton, R.L., 1995. Incompressible Flow (2nd ed.). John Wiley and Sons, New York.

Potts, J.R., Crowther, W.J. 2000. The flow over a rotating disc-wing. In Proceedings of
  the RAeS Aerodynamics Research Conference Proceedings, London, United
  Kingdom.

Potts, J.R., Crowther, W.J. 2001. Flight control of a spin stabilised axi-symmetric disc-
  wing. In Proceedings of the 39th Aerospace Sciences Meeting, Reno, Nevada,
  USA.

Potts, J.R., Crowther, W.J. 2002. Frisbee Aerodynamics AIAA Paper 2002-3150. In
  Proceedings of the 20th AIAA Applied Aerodynamics Conference, St. Louis,
  Missouri.

Pozzy, T. (2002, Winter). Getting More Distance: How the Pros Do It. *Disc Golf World
  News*.

Putnam, C.A., 1993. Sequential motions of body segments in striking and throwing skills: descriptions and explanations. J. Biomechanics 26, 125-135.

Roddick, D., 1980. Frisbee disc basics. Prentice-Hall, Englewood Cliffs, New Jersey.

Schuurmans, M., 1990. Flight of the Frisbee. New Scientist 127(July 28,1727), 37-40.

Shapiro, R., 1978. Direct linear transformation method for three-dimensional cinematography. Research Quarterly 49(197-205).

Soong, T.C., 1976. The dynamics of discus throw. Journal of Applied Mechanics 98, 531-536.

Sprigings, E., Marshall, R., Elliott, B., Jennings, L., 1994. A three-dimensional kinematic method for determining the effectiveness of arm segment rotations in producing racquet-head speed. J. Biomechanics 27, 245-254.

Stilley, G.D. (1972). Aerodynamic analysis of the self sustained flair. RDTR no 199, Naval Ammunition Depot. Crane Indiana.

Stilley, G.D., Carstens, D.L. 1972. Adaptation of Frisbee flight principle to delivery of special ordnance. AIAA Paper 72-982. In Proceedings of the 2nd Atmospheric Flight Mechanics Conference, Palo Alto, California.

Tips, C., 1977. Frisbee by the masters. Celestial Arts, Millbrae, California.

VanderHelm, F.C.T., 1994. Analysis of the kinematic and dynamic behavior of the shoulder mechanism. J. Biomechanics 27, 551-569.

Veeger, H.E.J., van der Helm, F.C.T., van der Woude, L.H.V., Pronk, G.M., Rozendal, R.H., 1991. Inertia and muscle contraction parameters for musculoskeletal modelling of the shoulder mechanism. J. Biomechanics 24, 615-629.

Yasuda, K., 1999. Flight and Aerodynamic Characteristics of a Flying Disk. Japanese

Society Aero. Space Science 47(547), 16-22 (in Japanese).

Appendix - Computer Programs

Appendix – A – simulate_flight.m

```
%%%%%%%%%%%%%%%%%%%%%%%%%%%%%%%%%%%%%%%%%%%%%%%%%%%%%
%% File:    simulate_flight.m
%% By:      Sarah Hummel
%% Date:    July 2003
%%
%% This MATLAB program allows the simulation of a single frisbee flight
%% given initial conditions and a set of aerodynamic coefficients.
%% Calls subroutine discfltEOM.m, the equations of motion for the frisbee.
%% Inertial xyz coordinates = forward, right and down
%%
%%   before executing code (as described below):
%% 1) specify value for "CoefUsed"
%% 2) specify which values for the damping coefficients, use long flight or short
%%    flight values.
%% 3) specify Simulation set of initial conditions: thetao, speedo, betao, and po
%% 4) specify which "x0" command to use
%% 5) specify values for "tfinal" and "nsteps"
%%
%%%%%%%%%%%%%%%%%%%%%%%%%%%%%%%%%%%%%%%%%%%%%%%%%%%%%
clear
format short

global m g Ia Id A d rho
global CLo CLa CDo CDa CMo CMa CRr
global CL_data CD_data CM_data CRr_rad CRr_AdvR CRr_data
global CMq CRp CNr

%%%%%%%%%%%%%%%%%%%%%%%%%%%%%%%%%%%%%%%%%%%%%%%%%%%%%
%% Set "CoefUsed" = 1 OR 2
%% This chooses the values of coefficients (specifies a set of if/then statements)
%% to use for CLo CLa CDo CDa CMo CMa CRr.
%% CoefUsed = 1 ... choose for using estimated short flights lift, drag, moment coefficients
%% CoefUsed = 2 ... choose for using Potts and Crowther (2002) lift, drag, moment coefficients

CoefUsed=2

%%%%%%%%%%%%%%%%%%%%%%%%%%%%%%%%%%%%%%%%%%%%%%%%%%%%%
%%  define non-aerodynamic parameters

m = 0.175                 % Kg
g = 9.7935                % m/s^2
A = 0.057                 % m^2
d = 2*sqrt(A/pi)          % diameter
rho = 1.23                % Kg/m^3
Ia  = 0.002352            % moment of inertia about the spinning axis
Id  = 0.001219            % moment of inertia about the planar axis'
```

81

```
%%%%%%%%%%%%%%%%%%%%%%%%%%%%%%%%%%%%%%%%%%%%%%%%%%%
%%  THE THREE ESTIMATED COEFFICIENTS

%CMq= -0.005,    CRp =-0.0055,   CNr =        0.0000071     % short (three) flights
 CMq= -1.44E-02       , CRp =-1.25E-02, CNr = -3.41E-05      % long flight f2302

%%%%%%%%%%%%%%%%%%%%%%%%%%%%%%%%%%%%%%%%%%%%%%%%%%%
%%  THE seven COEFFICIENTS estimated from three flights
CLo=  0.3331;
CLa=  1.9124;
CDo=  0.1769;
CDa=  0.685;
CMo= -0.0821;
CMa=  0.4338;
CRr=  0.00171;           % for nondimensionalization = sqrt(d/g), magnitude of CRr changes
                         % with nondimensionalization

%%%%%%%%%%%%%%%%%%%%%%%%%%%%%%%%%%%%%%%%%%%%%%%%%%%
%%  THE seven COEFFICIENTS from Potts and Crowther (2002)
%%  CL =[   rad         CL      deg]
CL_data=[ -0.1745     -0.2250 -10
          -0.05236       0       -3
           0           0.150   0
           0.08727     0.4500  5
           0.17453     0.7250  10
           0.26180     0.9750  15
           0.34907     1.2000  20
           0.43633     1.4500  25
           0.52360     1.6750  30];

%%  CD =[   rad        CD      deg]
CD_data=[ -0.1745     0.1500  -10
          -0.05236    0.0800  -3
           0          0.1000  0
           0.08727    0.1500  5
           0.1745     0.2600  10
           0.26180    0.3900  15
           0.3491     0.5700  20
           0.4363     0.7500  25
           0.5236     0.9200  30];

%%  CM =[     rad             CM          deg]
CM_data=[-0.174532925      -0.0380     -10
          -0.087266463      -0.0220     -5
          -0.052359878      -0.0140     -3
           0                -0.0060     0
           0.052359878      -0.0060     3
           0.104719755      -0.0020     6
           0.157079633       0.0000     9
           0.20943951        0.0100     12
```

```
          0.261799388              0.0220          15
          0.34906585               0.0440          20
          0.401425728              0.0600          23
          0.453785606              0.0840          26
          0.523598776              0.1100          30];

%%% CRr_deg=[-5        -4      -3      -2      -1      0      1      2      3      4
5      6        7       8       9       10      11     12     13     14     15     30   ]
CRr_rad = [-0.0873      -0.0698 -0.0524 -0.0349 -0.0175 0.0000 0.0175 0.0349 0.0524 0.0698
         0.0873 0.1047 0.1222 0.1396 0.1571 0.1745 0.1920 0.2094 0.2269 0.2443 0.2618
         0.5236];
CRr_AdvR= [2 1.04 0.69 0.35 0.17 0];

CRr_data =[-0.0172      -0.0192 -0.018  -0.0192 -0.018   -0.0172 -0.0172 -0.0168 -0.0188 -0.0164
         -0.0136 -0.01    -0.0104 -0.0108 -0.0084 -0.008   -0.008   -0.006   -0.0048 -0.0064 -0.008
-0.003
         -0.0112  -0.0132 -0.012  -0.0132 -0.012   -0.0112 -0.0112 -0.0108 -0.0128 -0.0104 -0.0096
         -0.0068 -0.0072 -0.0076 -0.0052 -0.0048 -0.0048 -0.0028 -0.0032 -0.0048 -0.0064 -0.003
         -0.0056  -0.0064 -0.0064 -0.0068 -0.0064 -0.0064 -0.0052 -0.0064 -0.0028 -0.0028 -0.004
         -0.002   -0.004  -0.002  -0.0016  0        0        0        0        -0.002  -0.0048 -0.003
         -0.0012  -0.0016 -0.0004 -0.0028 -0.0016 -0.0016 -0.0004 0.0004 0.0004 0.0008 0.0004
0.0008  0.0012  0.0008  0.002    0.0028 0.0032 0.0024 0.0028 0.0004 -0.0012 -0.003
         -0.0012  -0.0012 -0.0016 -0.0016 -0.0012 -0.0004 0.0004 0.0008 0.0008 0.0016 0.0004
0.002    0.0004 0.0016 0.002    0.002    0.002    0.0012 0.0012  0     -0.0012 -0.003
         -0.0012  -0.0012 -0.0004 -0.0008 -0.0008 -0.0008 0.0004 0.0004 0.0004 0.0008 0.0004
0.0008 -0.0004   0        0        0.0004  0        0        0.0004 -0.002  -0.0012 -0.003];

%%%%%%%%%%%%%%%%%%%%%%%%%%%%%%%%%%%%%%%%%%%%%%%%%%
%%  angle and angular velocities in rad and rad/sec respectively
%%  phi   = angle about the x axis        phidot         = angular velocity
%%  theta = angle about the y axis        thetadot       = angular velocity
%%  gamma = angle about the z axis        gd(gammadot)  = angular velocity

%%  For reference, two sets of previously used initial conditions...
%%  Long flight (f2302) release conditions:
%%      thetao = 0.211;  speedo = 13.5;  betao = 0.15;  gd=54
%%  Common release conditions:
%%      thetao = 0.192;  speedo = 14;      betao = 0.105; gd=50

%%  Define Simulation set initial conditions, enter your choosen values here:
     thetao =  .192    % initial pitch angle
     speedo = 13.7;          % magnitude, m/sec
     betao  = .105     % flight path angle in radians between velocity vector and horizontal
     gd=50;          % initial spin

%%%%%%%%%%%%%%%%%%%%%%%%%%%%%%%%%%%%%%%%%%%%%%%%%%%
alphao = thetao - betao         % inital alpha
vxo = speedo * cos(betao)       % velocity component in the nx direction
vzo = -(speedo * sin(betao))    % velocity component in the nz direction
                                %    (note: nz is positive down)
```

```
%%%%%%%%%%%%%%%%%%%%%%%%%%%%%%%%%%%%%%%%%%%%%%%
%% x0= vector of initial conditions
%% x0= [  x    y    z vx vy vz  phi theta  phidot thetadot gd   gamma]
%% Specify the set of inital conditions to use:
%%     the first set of conditions is for a disc released:
%%             theta, speed, and spin as specified above (thetao, speedo, gd),
%%             1 meter above the ground, forward and right 0.001,
%%             no roll angle, no velocity in the the y direction
%%             and for positive alpha, disc is pitched up, with a neg. w component
%%   the second set is the long flight f2302 estimated initial conditions
%% First set:
%x0= [ 0.001 0.001 -1 vxo 0  vzo 0  thetao 0.001  0.001   gd 0   ]
%% Second set:
x0=[-9.03E-01 -6.33E-01 -9.13E-01 1.34E+01   -4.11E-01 1.12E-03 -7.11E-02 2.11E-01 ...
    -1.49E+01 -1.48E+00 5.43E+01 5.03E+00]


%%%%%%%%%%%%%%%%%%%%%%%%%%%%%%%%%%%%%%%%%%%%%%%
%% Enter values for tfinal and nsteps:
tfinal = 1.46;  % length of flight
nsteps = 292;   % number of time steps for data
tspan=[0:tfinal/nsteps:tfinal];
options=[]
%options = odeset('AbsTol', 0.000001,'RelTol', 0.00000001,'OutputFcn','odeplot');

%% Calls the ODE and integrate the frisbee equations of motions in the
%%   subroutine, discfltEOM.m
[t,x]=ode45(@discfltEOM,tspan,x0,options,CoefUsed);

%%%%%%%%%%%%%%%%%%%%%%%%%%%%%%%%%%%%%%%%%%%%%%%
%% Remaining commands are associated with creating plots of the output. A "v"
%% is put at the end of the variable to differentiate it from the variable
%% calculated in discfltEOM.m

%% give states names  .... v for view for making plots
vxv = x(:,4);
vyv = x(:,5);
vzv = x(:,6);
fv  = x(:,7);
thv = x(:,8);
stv = sin(thv);
ctv = cos(thv);
sfv = sin(fv);
cfv = cos(fv);
fdv = x(:,9);
thdv= x(:,10);
pv  = x(:,11);

velv = [vxv vyv vzv]; %expressed in N
omegaD_N_inCv = [fdv.*ctv thdv  fdv.*stv + pv]; % expressed in c1,c2,c3
for i=1:size(t)
```

```matlab
    i=i;
    vmagv(i) = norm(velv(i,:)); % a nx1 row vector

    %% T_c_N=[ct      st*sf          -st*cf;
    %%         0       cf             sf;
    %%         st     -ct*sf         ct*cf]

    T_c_N=[    ctv(i)  stv(i)*sfv(i)      -stv(i)*cfv(i);
               0       cfv(i)             sfv(i);
               stv(i) -ctv(i)*sfv(i)      ctv(i)*cfv(i)];

    c3v(i,:)=T_c_N(3,:);                    % c3 expressed in N frame
    vc3v(i,:)=dot(velv(i,:),c3v(i,:));      % velocity (scalar) in the c3 direction
    vpv(i,:)= [velv(i,:)-vc3v(i,:).*c3v(i,:)]; % subtract c3 velocity component to get the
    %                                          velocity vector projected onto the plane
    %                                          of the disc, expressed in N
    vpmagv(i) = norm(vpv(i,:));
    uvpv(i,:)=vpv(i,:)/vpmagv(i);
    ulatv(i,:)=cross(c3v(i,:)',uvpv(i,:)')'; % unit vector perp. to v and c3, points right
    alphav(i) = atan(vc3v(i,:)/norm(vpv(i,:)));
    omegaD_N_inNv(i,:) = (T_c_N'*omegaD_N_inCv(i,:)')'; % expressed in n1,n2,n3

    omegavpv(i,:) = dot(omegaD_N_inNv(i,:),uvpv(i,:));    %omega about vp axis
    omegalatv(i,:) = dot(omegaD_N_inNv(i,:),ulatv(i,:));
    omegaspinv(i,:)= dot(omegaD_N_inNv(i,:),c3v(i,:));

end     %for i=1:size(t)

    Adpv = A*rho*vmagv.*vmagv/2;
    wuns=ones(size(alphav));
    AdvRv=d*omegaspinv/2./vmagv';

if   CoefUsed==1 % using short flights coefficients
    alphaeq= -CLo/CLa  % this is angle of attack at zero lift
   CLv = CLo*ones(size(alphav)) + CLa*alphav;
   CDv = CDo*ones(size(alphav)) + CDa*(alphav-alphaeq*ones(size(alphav))).*...
       (alphav-alphaeq*ones(size(alphav)));
   CMv = CMo*wuns + CMa*alphav;
   CRrv=CRr;
   %CRrv= CRr*d*omegaspinv/2./vmagv';
   %CRrv= CRr*sqrt(d/g)*omegaspinv;
   % above line produces NaN, so leave it in Mvp equation

   %Mvp = Adp*d* (CRrv*d*omegaspin/2/vmag + CRp*omegavp)*uvp;    % expressed in N
   Mvpv = Adpv*d* (sqrt(d/g)*CRrv*omegaspinv + CRp*omegavpv)*uvpv; % Roll moment
end     % if   CoefUsed==1 % using short flights coefficients

if   CoefUsed==2 % using Potts and Crowther (2002) coefficients
   %% interpolation of Potts and Crowther (2002) data
   CLv  = interp1(CL_data(:,1), CL_data(:,2), alphav,'spline');
   CDv  = interp1(CD_data(:,1), CD_data(:,2), alphav,'spline');
```

```
    CMv = interp1(CM_data(:,1), CM_data(:,2), alphav,'spline');
    CRrv = interp2(CRr_rad,CRr_AdvR,CRr_data,alphav,AdvRv,'spline');
    Mvpv = Adpv'*d.* (CRrv'  + CRp*omegavpv);              % Roll moment
end      % CoefUsed==2 % using potts coefficients

liftv=CLv.*Adpv;
dragv=CDv.*Adpv;

Mlatv = Adpv'*d.* (CMv' + CMq*omegalatv);   % Pitch Moment
Mspinv= [CNr*(fdv.*stv +pv)] ;            % Spin Down Moment

%%  Plot four subplots in one figure, the force and moments of the simulations
figure(1)
   clf
   subplot(2,2,1),plot(t,liftv)
       title('Liftv')
   subplot(2,2,2),plot(t,dragv)
       title('Dragv')
   subplot(2,2,3),plot(t,Mvpv,t,Mlatv)
      title(' Mvpv, Mlatv')
       xlabel('time(sec)')
   subplot(2,2,4),plot(t,Mspinv)
      title(' Mspinv')
      xlabel('time(sec)')

   veloc=sqrt(x(:,4).^2 +x(:,5).^2 +x(:,6).^2);
   mechenrgy=m*(-2*g*x(:,3) + x(:,4).^2 +x(:,5).^2 +x(:,6).^2) /2;
   Ho = mechenrgy/m/g;

figure(2)
   plot(t,mechenrgy,t,veloc,'.',t,Ho,t,AdvRv);
   legend('mechenrgy','vel','Ho','AdvRv')
   xlabel('time(sec)')

figure(3)
   plot(t,alphav)
   title('Angle of Attack, \alpha')
   xlabel('time(sec)')
   ylabel('(rad)')
   grid

%%  Plot four subplots in one figure, the states
figure(4)
subplot(2,2,1),plot(t,x(:,1),'k-',t,x(:,2),'k--',t,x(:,3),'k:','LineWidth',2)
       set(gca,'LineWidth',1);
       set(gca,'FontName','arial');
       set(gca,'FontSize',11);
               %xlabel('Time (sec)')
        ylabel('position (m)')
        legend('x','y','z');
       %axis tight
```

```
          %Ylim([-2 16])
          grid

subplot(2,2,2),plot(t,x(:,4),'k-',t,x(:,5),'k--',t,x(:,6),'k:','LineWidth',2)
           set(gca,'LineWidth',1);
          set(gca,'FontName','arial');
          set(gca,'FontSize',11);
          %xlabel('Time (sec)')
           ylabel('velocity (m/sec)')
           %title('Velocity of CM')
           legend('x\prime','y\prime','z\prime');
          %axis tight
          %Ylim([-2 14])
          %set(gca,'YTickLabel',{});
          grid

subplot(2,2,3),plot(t,x(:,7),'k-',t,x(:,8),'k--','LineWidth',2)
           set(gca,'LineWidth',1);
          set(gca,'FontName','arial');
          set(gca,'FontSize',11);
          xlabel('time (sec)')
           ylabel('orientation (rad)')
          %title('Phi, Theta')
           %title('Disc plane orientation')
           legend('\phi','\theta');
          grid

subplot(2,2,4),plot(t,x(:,9),'k-',t,x(:,10),'k--',t,0.1*x(:,11),'k:','LineWidth',2)
                          set(gca,'LineWidth',1);
          set(gca,'FontName','arial');
          set(gca,'FontSize',11);
          xlabel('time (sec)')
           ylabel('angular velocity (rad/sec)')
           %title('Angular velocities')
           legend('\phi\prime','\theta\prime','0.1*\gamma\prime');
          grid
```

Appendix – B – discfltEOM.m

```
%%%%%%%%%%%%%%%%%%%%%%%%%%%%%%%%%%%%%%%%%%%%%%%%%%%
%%% File:   discfltEOM.m
%%% By:     Sarah Hummel
%%% Date:   July 2003
%%%%%%%%%%%%%%%%%%%%%%%%%%%%%%%%%%%%%%%%%%%%%%%%%%%

function xdot=discfltEOM(t,x,CoefUsed)

% Equations of Motion for the frisbee
% The inertial frame, xyz = forward, right and down

global m g Ia Id A d rho
global CLo CLa CDo CDa CMo CMa CRr
global CL_data CD_data CM_data CRr_rad CRr_AdvR CRr_data
global CMq CRp CNr

% x = [ x y z vx vy vz f th  fd  thd  gd gamma]
%      1 2 3 4 5 6 7 8  9  10  11  12

%%% give states normal names
vx = x(4);
vy = x(5);
vz = x(6);
f  = x(7);
th = x(8);
st = sin(th);
ct = cos(th);
sf = sin(f);
cf = cos(f);
fd = x(9);
thd= x(10);
gd = x(11);

%%% Define transformation matrix
%%% [c]=[T_c_N] * [N]
T_c_N=[ct st*sf -st*cf; 0 cf sf; st -ct*sf ct*cf];
%%% [d]=[T_d_N] * [N]
%T_d_N(1,:)=[cg*ct  sg*cf+sf*st*cg  sf*sg-st*cf*cg];
%T_d_N(2,:)=[ -sg*ct cf*cg-sf*sg*st sf*cg+sg*st*cf];
%T_d_N(3,:)=[ st -sf*ct cf*ct]

[evec,eval]=eig(T_c_N);
eigM1=diag(eval);
m1=norm(eigM1(1));
m2=norm(eigM1(2));
m3=norm(eigM1(3));

c1=T_c_N(1,:);     % c1 expressed in N frame
```

```
c2=T_c_N(2,:);      % c2 expressed in N frame
c3=T_c_N(3,:);      % c3 expressed in N frame

%%% calculate aerodynamic forces and moments
%%% every vector is expressed in the N frame
vel = [vx vy vz];           %expressed in N
vmag = norm(vel);

vc3=dot(vel,c3);            % velocity (scalar) in the c3 direction
vp= [vel-vc3*c3];          % subtract the c3 velocity component to get the velocity vector
                           % projected onto the plane of the disc, expressed in N

alpha = atan(vc3/norm(vp));
Adp = A*rho*vmag*vmag/2;

uvel  = vel/vmag;                    % unit vector in vel direction, expressed in N
uvp   = vp/norm(vp);                 % unit vector in the projected velocity direction, expressed in N
ulat  = cross(c3,uvp);               % unit vec perp to v and d3 that points to right, right?

%%% first calc moments in uvp (roll), ulat(pitch) directions, then express in n1,n2,n3
omegaD_N_inC = [fd*ct thd  fd*st+gd];          % expressed in c1,c2,c3
omegaD_N_inN = T_c_N'*omegaD_N_inC';     % expressed in n1,n2,n3

omegavp   = dot(omegaD_N_inN,uvp);
omegalat  = dot(omegaD_N_inN,ulat);
omegaspin = dot(omegaD_N_inN,c3);              % omegaspin = p1=fd*st+gd
AdvR= d*omegaspin/2/vmag ;                     % advanced ration

if   CoefUsed==1                % using short flights coefficients
   CL  = CLo + CLa*alpha;
   alphaeq = -CLo/CLa;          % this is angle of attack at zero lift
   CD  = CDo + CDa*(alpha-alphaeq)*(alpha-alphaeq);
   CM=CMo + CMa*alpha;

   %CRr= CRr*d*omegaspinv/2./vmagv';
   %CRr= CRr*sqrt(d/g)*omegaspinv;   % this line produces NaN, so leave it in Mvp equation
   %Mvp = Adp*d* (CRr*d*omegaspin/2/vmag  + CRp*omegavp)*uvp;  % expressed in N
   Mvp = Adp*d* (sqrt(d/g)*CRr*omegaspin  + CRp*omegavp)*uvp;        % expressed in N
end      % if   CoefUsed==1 % using short flights coefficients

if    CoefUsed==2 % using potts coefficients
%%% interpolation of Potts and Crowther (2002) data

   CL  = interp1(CL_data(:,1), CL_data(:,2), alpha,'spline'
   CD  = interp1(CD_data(:,1), CD_data(:,2), alpha,'spline');
   CM  = interp1(CM_data(:,1), CM_data(:,2), alpha,'spline');
   CRr = interp2(CRr_rad,CRr_AdvR,CRr_data,alpha,AdvR,'spline');
   Mvp = Adp*d* (CRr*  + CRp*omegavp)*uvp;                    % Roll moment, expressed in N
end      % if   CoefUsed==2 % using potts coefficients

lift  = CL*Adp;
```

```
drag  = CD*Adp;
ulift = -cross(uvel,ulat);              % ulift always has - d3 component
udrag = -uvel;
Faero = lift*ulift + drag*udrag;        % aero force in N
FgN   = [ 0 0 m*g]';                    % gravity force in N
F = Faero' + FgN;

Mlat  = Adp*d* (CM + CMq*omegalat)*ulat;        % Pitch moment expressed in N
Mspin = [0 0 +CNr*(omegaspin)];                 % Spin Down moment expressed in C
M = T_c_N*Mvp' + T_c_N*Mlat' + Mspin';          % Total moment expressed in C

% set moments equal to zero if wanted...
% M=[0 0 0];

% calculate the derivatives of the states
xdot = vel';
xdot(4)  = (F(1)/m);     %accx
xdot(5)  = (F(2)/m);     %accy
xdot(6)  = (F(3)/m);     %accz
xdot(7)  = fd;
xdot(8)  = thd;
xdot(9)  = (M(1) + Id*thd*fd*st - Ia*thd*(fd*st+gd) + Id*thd*fd*st)/Id/ct;
xdot(10) = (M(2) + Ia*fd*ct*(fd*st +gd) - Id*fd*fd*ct*st)/Id;
fdd=xdot(9);
xdot(11) = (M(3) - Ia*(fdd*st + thd*fd*ct))/Ia;
xdot(12) = x(11);
xdott=xdot';

% calculate angular momentum
H = [Id 0 0 ; 0 Id 0; 0 0 Ia]*omegaD_N_inC';

format long;
magH = norm(H);
format short;
state=x';
```

Appendix – C – throw10.al

%%%
%%% File: throw10.al
%%% By: Sarah Hummel
%%% Date: July 2003
%%%
%%
%% AUTOLEV code for frisbee right hand backhand frisbee throws
%% file with 10 constraint equations, 6 TORQUES

%// **
%//   POINT   LANDMARK   NOTES
%//   --
%//   ORIGIN   NONE   origin of the global (N) frame
%//   IJ   Inc. Jug.   origin of thorax (THOR) frame
%//   STERNUM   sternum   origin of clavicular (CLAV) frame
%//   ACCLAV   A-C Joint   origin of scapula (SCAP) frame
%//   HH   Cntr Hum Head   origin of humerus (HUMER) frame
%//   ANGACROM Anterior Angle   point on scapula
%//   TS   NONE REALLY   point on scapula's medial border
%//   INFANG   Inferior Angle   point on scapula
%//   CONTACT1   SCAP CONTACT POINT NEAR TS
%//   CONTACT2   SCAP CONTACT POINT NEAR INFANG
%//   AA   ACROMIAL ANGLE OF SCAPULA
%//   CONINS   Conoid Ins   insertion point of conoid lig on scapula
%//   CONORG   Conoid Org   origin of conoid lig on clav
%//
%//   Elbow   proximal articulation of the ulna (with the humerus)
%//   Wrist   distal articulation of the radius (with the carpels)
%//   PROXRAD   proximal articulation of the radius (with the humerus)
%//   DISULNA   distal articulation of the ulna with the radius
AUTORHS ON
AUTOZ on
OVERWRITE ON
NEWTONIAN N
Degrees off

POINTS ORIGIN, IJ, STERNUM, ACCLAV, ANGACROM, TS, INFANG, HH, ELBOW,
WRIST, DISULNA, PROXRAD
POINTS CONTACT1, CONTACT2, CONINS, CONORG

CONSTANTS IJST{3}, CPTS{3}, CPAI{3}, ACMEDIJST{3}, ACAA{3}, ACTS{3},
ACAI{3}, ACHH{3}
CONSTANTS CO{3}, CI{3}, ITHOR{3}, ICLAV{3}, ISCAP{3}, IHUM{3}, IHAND{3},
ECENTER{3}, A, B , C, G
CONSTANTS ELWR{3}, LCLAV, RCLAV, LHUM, LTHOR, LHAND
CONSTANTS HUMCENTER, CLAVCENTER, THORCENTER, HANDCENTER
CONSTANTS RADCENTER, ULNACENTER, LRAD, LULNA, IRAD{3}, IULNA{3}
CONSTANTS LEAXIS, LWAXIS

Constants Cp_C, Cp_Hy, Cp_Hz, Cp_F, Cp_Xo, Cp_calcXo
Constants Ce_C, Ce_Hy, Ce_Hz, Ce_F, Ce_Xo, Ce_calcXo
Constants Sp_C, Sp_Hy, Sp_Hz, Sp_Cy, Sp_Cz, Sp_F, Sp_Xo, Sp_calcXo
Constants Sl_C, Sl_Hy, Sl_Hz, Sl_Cy, Sl_Cz, Sl_F, Sl_Xo, Sl_calcXo
Constants St_C, St_Hy, St_Hz, St_Cy, St_Cz, St_F, St_Xo, St_calcXo

BODIES CLAV, SCAP, THOR, HUMER, HAND
BODIES RADIUS, ULNA

VARIABLES THETA{12}', PSI{2}', Q{2}', U{16}'
VARIABLES XTHETA{6}'
VARIABLES HMAG1, HMAG2, HMAG3, EMAG1, EMAG3, WMAG3

SPECIFIED PHI{3}", QTHOR{3}"

%// ******** Masses and Inertia for rigid bodies and T's for simulation *********
MASS CLAV=MASS_CLAV, SCAP=MASS_SCAP, THOR=MASS_THOR,
HUMER=MASS_HUMER, HAND=MASS_HAND
MASS RADIUS=MASS_RADIUS, ULNA=MASS_ULNA

INERTIA THOR, ITHOR1, ITHOR2, ITHOR3
INERTIA HUMER, IHUM1, IHUM2, IHUM3
INERTIA HAND, IHAND1, IHAND2, IHAND3
INERTIA RADIUS, IRAD1, IRAD2, IRAD3
INERTIA ULNA,IULNA1,IULNA2,IULNA3

Units G=m/s^2, T=secs, PHI{1:3}=rad, QTHOR{1:3}=m
Units THETA{1:12}=rad, PSI{1:2}=rad, Q{1:2}=m, U{1:14}=rad/s, U{15:16}=m/s
Units PSI{1:2}'=rad/s,Q{1:2}'=m/s, U{1:14}'=rad/s^2, U{15:16}'=m/s^2
Units ICLAV{1:3}=kg m^2, ISCAP{1:3}=kg m^2, IHUM{1:3}=kg m^2, IHAND{1:3}=kg m^2
Units LCLAV=m, RCLAV=m, LHUM=m, LTHOR=m, LHAND=m
Units LRAD=m, LULNA=m, IRAD{1:3}=kg m^2, IULNA{1:3}=kg m^2
Units LEAXIS=m, LWAXIS=m
Units HMAG1=N*m, HMAG2=N*m, HMAG3=N*m, EMAG1=N*m, EMAG3=N*m,
WMAG3=N*m
Units MASS_CLAV=kg, MASS_SCAP=kg, MASS_THOR=kg, MASS_HUMER=kg ,
MASS_HAND=kg
Units MASS_RADIUS=kg, MASS_ULNA=kg

INPUT   A   = 1.53000000000000E-01
INPUT   ACAA1   = 2.34514357016476E-02
INPUT   ACAA2   = -2.14623357172765E-02
INPUT   ACAA3   = -1.89619885588770E-02
INPUT   ACAI1   = -1.29807027137128E-01
INPUT   ACAI2   = -2.14623357172765E-02
INPUT   ACAI3   = -1.30729736514540E-01
INPUT   ACHH1   = 1.68273131171622E-02
INPUT   ACHH2   = 8.98723837185210E-03
INPUT   ACHH3   = -5.19034894409049E-02
INPUT   ACTS1   = -1.16526348249950E-01

```
INPUT      ACTS2           = -2.14623357172765E-02
INPUT      ACTS3           = -1.89619885588770E-02
INPUT      B               =  1.30000000000000E-01
INPUT      C               =  4.04200000000000E-01
INPUT      CI1             = -2.91109766490449E-02
INPUT      CI2             =  2.02823384045437E-02
INPUT      CI3             = -1.02294753697637E-02
INPUT      CO1             =  1.20135271196126E-01
INPUT      CO2             = -9.51058397995266E-03
INPUT      CO3             = -3.39716048537708E-04
INPUT      CPAI1           = -1.202607598873941e-01
INPUT      CPAI2           =  7.500500678916461e-02
INPUT      CPAI3           = -1.178078111191653e-01
INPUT      CPTS1           = -1.081839789957913e-01
INPUT      CPTS2           =  8.933773580982990e-02
INPUT      CPTS3           = -3.938013292146333e-03
%INPUT      ECENTER1        = 0%NOTNEEDED
%INPUT      ECENTER2        = 0         %NOTNEEDED
INPUT      ECENTER3        = -3.05391804509284E-01
INPUT      G               = -9.8
INPUT      HUMCENTER    =  0.5275

INPUT      RADCENTER    =  0.3926
INPUT      ULNACENTER  =  0.3926
INPUT      HANDCENTER =  .4

INPUT      IRAD1           = 1/2*0.00026
INPUT      IRAD2           = 1/2*0.00824
INPUT      IRAD3           = 1/2*0.00824
INPUT      IULNA1          = 1/2*0.00026
INPUT      IULNA2          = 1/2*0.00824
INPUT      IULNA3          = 1/2*0.00824
INPUT      IHUM1           = 0.00132
INPUT      IHUM2           = 0.01432
INPUT      IHUM3           = 0.01432
INPUT      IHAND1          =  0.00018
INPUT      IHAND2          =  0.00062
INPUT      IHAND3          =  0.00062
INPUT      ITHOR1          = 1     %NOTNEEDED
INPUT      ITHOR2          = 1     %NOTNEEDED
INPUT      ITHOR3          = 1     %NOTNEEDED
INPUT      IJST1           = 2.75000000000000E-02
INPUT      IJST2           = -2.42808751328559E-02
INPUT      IJST3           = 1.21572654319408E-02
INPUT      LHUM            = 0.345

INPUT      LRAD            = .27
INPUT      LULNA           = .27
INPUT      LTHOR           = 1     %not needed
INPUT      LEAXIS          = .0687
INPUT      LWAXIS          = .0573
```

```
INPUT        LHAND         = .11

INPUT        LCLAV         = 1.48380153659443E-01
INPUT        CLAVCENTER = 0.5
INPUT        THORCENTER = 0.5
INPUT        MASS_CLAV    = 0.3135
INPUT        MASS_SCAP    = 0.692
INPUT        MASS_HUMER = 1.72
INPUT        MASS_RADIUS = 1/2*1.04
INPUT        MASS_ULNA    = 1/2*1.04
% mass_hand = .46 + .175 (frisbee)
INPUT        MASS_HAND    = 0.46
INPUT        RCLAV         = 0.02


%// Inputs for the generalized coordinates as determined from initialcalc.al

INPUT        PSI1          = -1.28400385782876E+000
INPUT        PSI2          = -1.27336166627895E+000
INPUT        Q1            =  4.57426940582380E-003
INPUT        Q2            = -1.06754669122816E-001
INPUT        THETA4        =  5.27271090588841E-001
INPUT        THETA6        = -1.39799749848556E-001
INPUT        THETA3        =  5.17416813525056E-003

INPUT        THETA1        = -.3829
INPUT        THETA2        = -.109
INPUT        THETA5        = -.06859


%//Inputs for the Clavicle regression equations
INPUT        Cp_C          = 4.98
INPUT        Cp_Hy          = 0.12
INPUT        Cp_Hz          = 0.24
INPUT        Cp_F          = 0.01
INPUT        Cp_Xo          = 0.85
INPUT        Ce_C          = 3.91
INPUT        Ce_Hy          = 0.05
INPUT        Ce_Hz          = 0.12
INPUT        Ce_F          = 0.35
INPUT        Ce_Xo          = 0.49
%//
%//Inputs for the Scapula regression equations
INPUT        Sp_C          = 27.94
INPUT        Sp_Hy          = 0.07
INPUT        Sp_Hz          = 0.09
INPUT        Sp_Cy          = 0.78
INPUT        Sp_Cz          = 0.39
INPUT        Sp_F          = 0.32
INPUT        Sp_Xo          = 0.41
INPUT        Sl_C          = 6.97
INPUT        Sl_Hy          = 0.01
INPUT        Sl_Hz          = 0.22
```

```
INPUT          Sl_Cy          = 0.26
INPUT          Sl_Cz          = 0.9
INPUT          Sl_F           = 0.98
INPUT          Sl_Xo           = 0.26
INPUT          St_C           = 4.88
INPUT          St_Hy           = 0
INPUT          St_Hz           = 0.15
INPUT          St_Cy           = 0.27
INPUT          St_Cz           = 0.22
INPUT          St_F           = 0.71
INPUT          St_Xo           = 0.69
```

%// Inputs for regression equation that are not needed because they
%// dissappear when the derivative is taken.

```
%INPUT         Cp_calcXo       = 1
%INPUT         Ce_calcXo       = 1
%INPUT         Sp_calcXo        = 1
%INPUT         Sl_calcXo       = 1
%INPUT         St_calcXo       = 1
```

%// ***
%//   PHI IS A SPECIFIED QUANTITY
%// ***

DIRCOS(N,THOR,BODY321,PHI1,PHI2,PHI3)
ANGVEL(N,THOR,BODY321,PHI1,PHI2,PHI3)

%// ***
%//   THETA1 == HORIZONTAL ABDUCTION
%//   THETA2 == ABDUCTION (-)
%//   THETA3 == INTERNAL(-)/EXT.(+) ROTATION
%// ***

DIRCOS(THOR,CLAV,BODY321,THETA1,THETA2,THETA3)
W_CLAV_THOR> = U1*CLAV1> + U2*CLAV2> + U3*CLAV3>
KINDIFFS(THOR,CLAV,BODY321,THETA1,THETA2,THETA3)

%// ***
%//   THETA4 == SCAPULAR TWIST (CCW FROM TOP IS +),
%//   THETA5 == ROTATION (CW FROM REAR IS +)
%//   THETA6 == SCAPULAR TILT
%// ***

DIRCOS(THOR,SCAP,BODY321,THETA4,THETA5,THETA6)
W_SCAP_THOR> = U4*SCAP1> + U5*SCAP2> + U6*SCAP3>
KINDIFFS(THOR,SCAP,BODY321,THETA4,THETA5,THETA6)

%// ***
%//   THETA7 == HORIZONTAL ABDUCTION,
%//   THETA8 == ABDUCTION (-)

95
```

```
%//      THETA9 == INTERNAL(-)/EXT.(+)  ROTATION
%// *********************************************************

DIRCOS(THOR,HUMER,BODY321,THETA7,THETA8,THETA9)
W_HUMER_THOR> = U7*HUMER1> + U8*HUMER2> + U9*HUMER3>
KINDIFFS(THOR,HUMER,BODY321,THETA7,THETA8,THETA9)

%  define the positions
P_ORIGIN_IJ> = QTHOR1*N1> + QTHOR2*N2> + QTHOR3*N3>
P_IJ_STERNUM> = IJST1*THOR1> + IJST2*THOR2> + IJST3*THOR3>
P_STERNUM_ACCLAV> = LCLAV*CLAV1>
P_ACCLAV_ANGACROM> = ACAA1*SCAP1> + ACAA2*SCAP2> + ACAA3*SCAP3>
P_ACCLAV_TS> = ACTS1*SCAP1> + ACTS2*SCAP2> + ACTS3*SCAP3>
P_ACCLAV_INFANG> = ACAI1*SCAP1> + ACAI2*SCAP2> + ACAI3*SCAP3>
P_ACCLAV_HH> = ACHH1*SCAP1> + ACHH2*SCAP2> + ACHH3*SCAP3>
P_ACCLAV_CONTACT1> = CPTS1*SCAP1> + CPTS2*SCAP2> + CPTS3*SCAP3>
P_ACCLAV_CONTACT2> = CPAI1*SCAP1> + CPAI2*SCAP2> + CPAI3*SCAP3>
P_HH_ELBOW> = LHUM*HUMER1>

%// "Elbow" is the proximal articulation of the ulna (with the humerus)
%// "Wrist" is the distal articulation of the radius (with the carpels)
%// "PROXRAD" is the proximal articulation of the radius (with the humerus)
%// "DISULNA" is the distal articulation of the ulna with the radius
%
P_ELBOW_PROXRAD> = LEAXIS*ULNA3>
P_ELBOW_DISULNA> = LULNA*ULNA1>
P_PROXRAD_WRIST> =  LRAD*RADIUS1>
P_DISULNA_PROXRAD>=P_DISULNA_PROXRAD>
PSaxis> = unitvec(P_DISULNA_PROXRAD>)

P_STERNUM_CLAVO> = LCLAV * CLAVCENTER *CLAV1>
P_IJ_THORO> = -LTHOR * THORCENTER * THOR3> %NOTNEEDED?
P_HH_HUMERO> =  LHUM * HUMCENTER  * HUMER1>
P_PROXRAD_RADIUSO>  = LRAD  * RADCENTER  * RADIUS1>
P_ELBOW_ULNAO> = LULNA * ULNACENTER * ULNA1>

P_WRIST_HANDO> = LHAND * HANDCENTER * HAND1>

%// *********************************************************
%//   DEGREES OF FREEDOM of FOREARM AND HAND
%//      THETA10 == ELBOW FLEXION(+)/EXTENSION (-)
%//      THETA11 == SUPINATION (-)/ PRONATION (+)
%//      THETA12 == WRIST FLEXION(+)/EXTENSION (-)
%// *********************************************************

SIMPROT(HUMER,ULNA,3,THETA10)
SIMPROT(ULNA,RADIUS,PSaxis>,THETA11)
W_ULNA_HUMER>  = U10*ULNA3>
W_RADIUS_ULNA> = U11*PSaxis>

express(P_ELBOW_PROXRAD> ,n)
```

THETA10'=U10
THETA11'=U11

SIMPROT(RADIUS,HAND,3,THETA12)
W_HAND_RADIUS> = U12*HAND3>
THETA12'=U12

%// define inertia of scapula and clavicle
%// Scapula is modeled as a right triangle with legs the mags of AATS and TSAI
LEG1 = MAG(P_ANGACROM_TS>)
LEG2 = MAG(P_TS_INFANG>)
TEMPSCAP = MASS_SCAP/18
P_ACCLAV_SCAPO> = -(2 * LEG1 * SCAP1>)/3 - (LEG2 * SCAP3>)/3

ISCAP1 = TEMPSCAP*LEG2*LEG2
ISCAP2 = TEMPSCAP*LEG1*LEG1 + TEMPSCAP*LEG2*LEG2
ISCAP3 = TEMPSCAP*LEG1*LEG1
INERTIA SCAP,ISCAP1,ISCAP2,ISCAP3,0,0,(-TEMPSCAP*LEG1*LEG2)/2

ICLAV1 = 0.5 * MASS_CLAV * RCLAV * RCLAV
ICLAV2 = (MASS_CLAV / 12) * ((3 * RCLAV * RCLAV) + (LCLAV * LCLAV))
ICLAV3 = ICLAV2
INERTIA CLAV,ICLAV1,ICLAV2,ICLAV3

% define velocities
V_ORIGIN_N> = 0>
V_IJ_THOR> = 0>
V_IJ_N> = dt(P_ORIGIN_IJ>,N)
% which equals -->V_IJ_N>= QTHOR1'*N1>+QTHOR2'*N2>+QTHOR3'*N3>
V_STERNUM_THOR> = 0>
V2PTS(THOR,CLAV,STERNUM,ACCLAV)
V2PTS(THOR,SCAP,ACCLAV,TS)
V2PTS(THOR,SCAP,ACCLAV,INFANG)
V2PTS(THOR,SCAP,ACCLAV,CONTACT1)
V2PTS(THOR,SCAP,ACCLAV,CONTACT2)
EXPRESS(V_TS_THOR>,THOR)
EXPRESS(V_INFANG_THOR>,THOR)
EXPRESS(V_CONTACT1_THOR>,THOR)
EXPRESS(V_CONTACT2_THOR>,THOR)

PSI1' = U13
PSI2' = U14
Q1' = U15
Q2' = U16
%// ********* PTS> is the vector from the sternum to the first medial border
%// ********* contact point expressed in terms of PS1 and Q1 in the THOR frame.
%// ********* It is used to derive the constraints.
%// Introduce the ellipsoid-shaped thorax here
%// PMEDB>=A*COS(THETA7)*N1> + (B*SIN(THETA7))*N2> + Q1*N3>
AA1 = (A*A - (A*(Q1-ECENTER3)/C)^2)^0.5

BB1 = (B*B - (B*(Q1-ECENTER3)/C)^2)^0.5
PTS>=(AA1*COS(PSI1) + ECENTER1)*THOR1> + (BB1*SIN(PSI1) +
ECENTER2)*THOR2> + Q1*THOR3>
VTS>=explicit(DT(PTS>,THOR))

%// ********* PINFANG> is the vector from the sternum to the second medial border
%// ********* contact point expressed in terms of PSI2 and Q2 in the THOR frame.
%// ********* It is used to derive the constraints.
AA2 = (A*A - (A*(Q2-ECENTER3)/C)^2)^0.5
BB2 = (B*B - (B*(Q2-ECENTER3)/C)^2)^0.5
PINFANG>=(AA2*COS(PSI2) + ECENTER1)*THOR1> + (BB2*SIN(PSI2) +
ECENTER2)*THOR2> + Q2*THOR3>
VINFANG>=explicit(DT(PINFANG>,THOR))

%// ********* The constraint equations ***********************
DEPENDENT[1] = DOT(VTS>, THOR1>) - DOT(V_CONTACT1_THOR>, THOR1>)
DEPENDENT[2] = DOT(VTS>, THOR2>) - DOT(V_CONTACT1_THOR>, THOR2>)
DEPENDENT[3] = DOT(VTS>, THOR3>) - DOT(V_CONTACT1_THOR>, THOR3>)
DEPENDENT[4] = DOT(VINFANG>, THOR1>) - DOT(V_CONTACT2_THOR>, THOR1>)
DEPENDENT[5] = DOT(VINFANG>, THOR2>) - DOT(V_CONTACT2_THOR>, THOR2>)
DEPENDENT[6] = DOT(VINFANG>, THOR3>) - DOT(V_CONTACT2_THOR>, THOR3>)
%
%// Constraint equations that assume the conoid ligament is rigid
P_STERNUM_CONORG> = CO1*CLAV1> + CO2*CLAV2> + CO3*CLAV3>
P_ACCLAV_CONINS> = CI1*SCAP1> + CI2*SCAP2> + CI3*SCAP3>
EXPRESS(P_ACCLAV_CONINS>, THOR)
EXPRESS(P_ACCLAV_CONINS>, CLAV)
MYANGLE = ATAN(DOT(P_CONORG_CONINS>,CLAV3>) /
DOT(P_CONORG_CONINS>,CLAV2>))
DEPENDENT[7] = explicit(DT(MYANGLE),U1,U2,U3,U4,U5,U6)
%
%// Regression equations for the remaining clav and scap DOF
%XTHETA1 =Cp_C + THETA7*Cp_HY + ABDUCTION*Cp_HZ + Cp_F*1 +
Cp_XO*Cp_CALCXO
%XTHETA2 =Ce_C + THETA7*Ce_HY + ABDUCTION*Ce_HZ + Ce_F*1 +
Ce_XO*Ce_CALCXO
%XTHETA5 =Sl_C + THETA7*Sl_HY + ABDUCTION*Sl_HZ + Sl_F*1 +
Sl_XO*Sl_CALCXO +Sl_Cy*xtheta1 +Sl_Cz *xtheta2
%XTHETA1'=DT(XTHETA1,N)
%XTHETA2'=DT(XTHETA2,N)
%XTHETA5'=DT(XTHETA5,N)
%regress1=explicit(xtheta1')
%regress2=explicit(xtheta2')
%regress5=explicit(xtheta5')
%Dependent[8] =explicit(regress1-theta1')
%Dependent[9] =explicit(regress2-theta2')
%Dependent[10]=explicit(regress5-theta5')

%//%%%%%%%
%//replacing the above with the equations per Cote's suggestions on 8-27

%XTHETA1' = 0.12 *THETA7' + 0.24 *THETA8' - THETA1'
%XTHETA1' = CP_HY*THETA7' + CP_HZ*THETA8' - THETA1'

%XTHETA2' = 0.05*THETA7' + 0.12*THETA8' - THETA2'
%XTHETA2' = CE_HY*THETA7' + CE_HZ*THETA8'- THETA2'

%XTHETA5' =   0.01 *THETA7' + 0.22 *THETA8' + 0.26 *THETA1' + 0.9 *THETA2' -
THETA5'
%XTHETA5' =   SL_HY*THETA7' + SL_HZ *THETA8' + SL_CY *XTHETA1' +
SL_CZ*XTHETA2' - THETA5'

%//%%%%%%%%%%%%%% writing equations to match the excel equations exactly!
%// All coefficients are input with positive values.
%XTHETA1' = 0.12 *THETA7' + 0.24 *THETA8' - THETA1'
XTHETA1'= CP_HY*THETA7' + CP_HZ*THETA8' - THETA1'

%XTHETA2' = 0.05*THETA7' + 0.12*THETA8' - THETA2'
XTHETA2'= CE_HY*THETA7' + CE_HZ*THETA8'- THETA2'

%XTHETA5' = 0.01 *THETA7' + 0.22 *THETA8' + 0.26 *THETA1' - 0.9 *THETA2' -
THETA5'
XTHETA5'= SL_HY*THETA7' + SL_HZ *THETA8' + SL_CY *THETA1' -
SL_CZ*THETA2' - THETA5'

Dependent[8] = explicit(xtheta1')
Dependent[9] = explicit(xtheta2')
Dependent[10]= explicit(xtheta5')

CONSTRAIN(MINORS,DEPENDENT[U13;U4;U15;U14;U6;U16;U1;U2;U3;U5])

%// ********* Velocities **************
%//V2PTS(N,THOR,ORIGIN,IJ)

V2PTS(N,THOR,IJ,STERNUM)
V2PTS(N,THOR,IJ,THORO)
V2PTS(N,CLAV,STERNUM,CLAVO)
V2PTS(N,CLAV,STERNUM,ACCLAV)
V2PTS(N,SCAP,ACCLAV,SCAPO)
V2PTS(N,SCAP,ACCLAV,HH)

V2PTS(N,HUMER,HH,HUMERO)
V2PTS(N,HUMER,HH,ELBOW)
V2PTS(N,ULNA,ELBOW,ULNAO)
V2PTS(N,RADIUS,ELBOW,RADIUSO)
V2PTS(N,RADIUS,ELBOW,WRIST)
V2PTS(N,HAND,WRIST,HANDO)

%// ********* Accelerations ***********
ALF_THOR_N> = DT(W_THOR_N>,N)
ALF_CLAV_THOR>=DT(W_CLAV_THOR>,THOR)
%//ALF_SCAP_CLAV>=DT(W_SCAP_CLAV>,CLAV)

```
ALF_SCAP_THOR>=DT(W_SCAP_THOR>,THOR)
ALF_HUMER_THOR> = DT(W_HUMER_THOR>,THOR)
ALF_ULNA_HUMER> = DT(W_ULNA_HUMER>,HUMER)
ALF_RADIUS_ULNA> = DT(W_RADIUS_ULNA>,ULNA)
ALF_HAND_RADIUS> = DT(W_HAND_RADIUS>,RADIUS)

A_IJ_N> = DT(V_IJ_N>,N)
% which is equal to A_IJ_N> = QTHOR1"*N1>+QTHOR2"*N2>+QTHOR3"*N3>
A2PTS(N,THOR,IJ,STERNUM)
A2PTS(N,THOR,IJ,THORO)
A2PTS(N,CLAV,STERNUM,CLAVO)
A2PTS(N,CLAV,STERNUM,ACCLAV)
A2PTS(N,SCAP,ACCLAV,SCAPO)
A2PTS(N,SCAP,ACCLAV,HH)
A2PTS(N,HUMER,HH,HUMERO)
A2PTS(N,HUMER,HH,ELBOW)
A2PTS(N,HAND,WRIST,HANDO)
A2PTS(N,ULNA,ELBOW,ULNAO)
A2PTS(N,RADIUS,ELBOW,RADIUSO)
A2PTS(N,RADIUS,ELBOW,WRIST)


%// ********* Apply the force of gravity at the C.M. of each rigid body *********
GRAVITY(G*N3>)

%// ***********************************************************************
%// JOINT TORQUES
%// ***********************************************************************
SHOULDERTORQUE>=HMAG1*HUMER1>+HMAG2*HUMER2>+HMAG3*HUMER3>
ELBOWTORQUE>=EMAG3*ULNA3>
FARMTORQUE> = EMAG1*PSaxis>
WRISTTORQUE>=WMAG3*RADIUS3>

TORQUE(THOR/HUMER, SHOULDERTORQUE>)
TORQUE(HUMER/ULNA, ELBOWTORQUE>)
TORQUE(ULNA/RADIUS, FARMTORQUE>)
TORQUE(RADIUS/HAND, WRISTTORQUE>)


%// ********* My main man KANE!!!!!! *********
ZERO=FR()+FRSTAR()
explicit(zero,HMAG1,HMAG2,HMAG3,EMAG1,EMAG3,WMAG3)

Output T, PSI1, PSI2, Q1, Q2, MYANGLE, Theta1,Theta2,Theta3,theta4,Theta5,theta6
OUTPUT T, U1, U2, U3, U4, U5, U6, U13, U14, U15, U16
OUTPUT T, U7, U8, U9, U10, U11, U12
OUTPUT T, HMAG1,HMAG2,HMAG3,EMAG1,EMAG3,WMAG3

THETA1pp = DT(THETA1')
THETA2pp = DT(THETA2')
THETA3pp = DT(THETA3')
```

THETA4pp = DT(THETA4')
THETA5pp = DT(THETA5')
THETA6pp = DT(THETA6')

OUTPUT T, THETA1pp,THETA2pp,THETA3pp,THETA4pp,THETA5pp,THETA6pp
OUTPUT T, U1', U2', U3', U4', U5', U6', U13', U14', U15', U16'
Output T, Theta7,Theta8,Theta9,theta10,Theta11,theta12

P_IJ>=EXPRESS(P_ORIGIN_IJ>, N)
P_IJNx=DOT(N1>,P_IJ>)
P_IJNy=DOT(N2>,P_IJ>)
P_IJNz=DOT(N3>,P_IJ>)
P_IJx=DOT(THOR1>,P_IJ>)
P_IJy=DOT(THOR2>,P_IJ>)
P_IJz=DOT(THOR3>,P_IJ>)

P_HH>=EXPRESS(P_IJ_HH>, THOR)
P_HHx=DOT(THOR1>,P_HH>)
P_HHy=DOT(THOR2>,P_HH>)
P_HHz=DOT(THOR3>,P_HH>)

P_HUMERO>=EXPRESS(P_IJ_HUMERO>, THOR)
P_HUMEROx=DOT(THOR1>,P_HUMERO>)
P_HUMEROy=DOT(THOR2>,P_HUMERO>)
P_HUMEROz=DOT(THOR3>,P_HUMERO>)

P_ELBOW>=EXPRESS(P_IJ_ELBOW>, THOR)
P_ELBOWx=DOT(THOR1>,P_ELBOW>)
P_ELBOWy=DOT(THOR2>,P_ELBOW>)
P_ELBOWz=DOT(THOR3>,P_ELBOW>)

P_rado>=EXPRESS(P_IJ_RADIUSO>, THOR)
P_RADOX=DOT(THOR1>,P_RADO>)
P_RADOY=DOT(THOR2>,P_RADO>)
P_RADOZ=DOT(THOR3>,P_RADO>)

P_ULNAO>=EXPRESS(P_IJ_ULNAO>, THOR)
P_ULNAOx=DOT(THOR1>,P_ULNAO>)
P_ULNAOy=DOT(THOR2>,P_ULNAO>)
P_ULNAOz=DOT(THOR3>,P_ULNAO>)

P_WRIST>=EXPRESS(P_IJ_WRIST>, THOR)
P_WRISTx=DOT(THOR1>,P_WRIST>)
P_WRISTy=DOT(THOR2>,P_WRIST>)
P_WRISTz=DOT(THOR3>,P_WRIST>)

P_HANDO>=EXPRESS(P_IJ_HANDO>, THOR)
P_HANDOX=DOT(THOR1>,P_HANDO>)
P_HANDOY=DOT(THOR2>,P_HANDO>)
P_HANDOZ=DOT(THOR3>,P_HANDO>)

```
P_CLAVO>=EXPRESS(P_IJ_CLAVO>, THOR)
P_CLAVOx=DOT(THOR1>,P_CLAVO>)
P_CLAVOy=DOT(THOR2>,P_CLAVO>)
P_CLAVOz=DOT(THOR3>,P_CLAVO>)

P_SCAPO>=EXPRESS(P_IJ_SCAPO>, THOR)
P_SCAPOX=DOT(THOR1>,P_SCAPO>)
P_SCAPOY=DOT(THOR2>,P_SCAPO>)
P_SCAPOZ=DOT(THOR3>,P_SCAPO>)

P_PROXRAD>=EXPRESS(P_IJ_PROXRAD>, THOR)
P_PROXRADx=DOT(THOR1>,P_PROXRAD>)
P_PROXRADy=DOT(THOR2>,P_PROXRAD>)
P_PROXRADz=DOT(THOR3>,P_PROXRAD>)

P_DISULNA>=EXPRESS(P_IJ_DISULNA>, THOR)
P_DISULNAX=DOT(THOR1>,P_DISULNA>)
P_DISULNAY=DOT(THOR2>,P_DISULNA>)
P_DISULNAZ=DOT(THOR3>,P_DISULNA>)

output T, P_CLAVOx, P_CLAVOy, P_CLAVOz, P_SCAPOx, P_SCAPOy, P_SCAPOz,
P_HHx, P_HHy, P_HHz, P_HUMEROx, P_HUMEROy, P_HUMEROz
OUTPUT T, P_ELBOWx, P_ELBOWy, P_ELBOWZ, P_PROXRADx, P_PROXRADy,
P_PROXRADz, P_DISULNAx, P_DISULNAy, P_DISULNAz
OUTPUT T, P_RADOx,P_RADOy, P_RADOz, P_ULNAOx, P_ULNAOy, P_ULNAOz,
P_WRISTx, P_WRISTy, P_WRISTz, P_HANDOx, P_HANDOy, P_HANDOz
output T, P_IJx, P_IJy, P_IJz, P_IJNx, P_IJNy, P_IJNz

CODE ALGEBRAIC(ZERO,HMAG1,HMAG2,HMAG3,EMAG1,EMAG3,WMAG3)
10v7.for,subs
```